ABSTRACT

Title: ATOMIZATION MODEL DEVELOPMENT FOR FIRE SUPPRESSION DEVICES

Di Wu, Master of Science, 2005

Directed By: Andre Marshall, Assistant Professor, Department of Fire Protection Engineering

The performance of water-based fire suppression systems is governed by the dispersion of the droplets in the spray. Characterization of the spray is essential for predicting and evaluating the performance of these suppression systems. The accuracy of the spray characterization is quite sensitive to the initial spray specification when using particle tracking method to model spray dispersion. An atomization model based on first principles has been developed for predicting the distributed properties for the initial spray. Inputs to this model include injector geometry, operating conditions, and suppressant fluid properties. This modeling approach has also been integrated with drop dispersion models in FDS 4.0 to characterize spray dispersion behavior. The effect of initial spray specification on spray dispersion behavior in a quiescent environment has also been addressed. The drop size predictions using the proposed atomization model have demonstrated favorable agreement with actual sprinkler spray measurements over a range of operating conditions.

ATOMIZATION MODEL DEVELOPMENT FOR FIRE SUPPRESSION DEVICES

By

Di Wu

Thesis submitted to the Faculty of the Graduate School of the
University of Maryland, College Park, in partial fulfillment
of the requirements for the degree of
Master of Science
2005

Advisory Committee:
Professor Andre Marshall, Chair
Professor Arnaud Trouve
Professor Peter B. Sunderland

Acknowledgements

This work is supported by the National Fire Sprinkler Association (NFSA). I wanted to thank the program manager Mr. Russell Fleming of NFSA for his support. I wanted to express my gratitude to Dr. Andre Marshall, my advisor, for his guidance, support and countless time to help me to complete this work.

I would also like to thank the rest of my thesis committee, Dr. Arnaud Trouve and Dr. Sunderland, I really appreciated your support. A special thanks to Dr. Richard Roby and Dr. Mike Klassen and all the other people in Combustion Science& Engineering, Inc. for expanding my knowledge.

In addition, I wanted to thank all the staff and graduate student in Fire Protection Department for their kindness and help in these two years, especially to Xiaobo Yao and Yi Wang.

Finally, I would like to thank my parents, their encouragement and support always gave me courage and confidence when I met difficulties. I also thank my boyfriend Lei Zhou, for his continuous support through out the completion of this work.

Table of Contents

List of Figures

Chapter 1: Introduction

1.1 Overview

Sprinklers are used extensively in a variety of fire protection applications. The simplicity and effectiveness of these devices have made them a popular fire suppression choice for many years. An advanced water suppression technology known as water mist also receives more interest since 1980s because of recent International Maritime Organisation (IMO) regulations which prohibits ozone-depleting Halons for fire suppression applications. The suppression performance of water mist technology is comparable to conventional sprinklers and the performance is achieved with relatively low water demands and less potential water damage. The basic suppression mechanisms for water based suppression are clearly understood, which are extraction of heat from the fire gases during drop vaporization and expansion, attenuation of heat feedback from the fire by absorption and to a lesser extent scattering of the thermal radiation by the spray , and the surface cooling by water vaporization on wet objectives. A recent comprehensive overview of water based fire suppression is provided in Grant et. Al. [1]. The performance of these suppression systems is primarily evaluated through full-scale spray dispersion tests and actual fire suppression tests. It is difficult to extrapolate the spray dispersion test performance to real fire scenarios because of the potential strong coupling between the fire and the spray. Alternatively, actual full-scale suppression tests are expensive making it difficult

to generate sufficient test statistics for proper evaluation of test results. Predictive models are needed to evaluate spray characteristics and to couple with fire models to predict suppression performance. Developments in CFD modeling make it possible to simulate the gas behavior of fires with a high degree of fidelity. However, before these tools can be used for fire suppression analysis, the detailed physics involved in spray atomization and spray dispersion must be clearly understood. Then the descriptive models for the spray can be implemented into CFD code to predict the performance of water based fire suppression systems. The strong coupling between the continuous phase (gas phase) and the dispersed phase (spray) makes accurate dispersed phase models essential for fire suppression analysis. Actually, the drop dispersion models are well defined for tracking the drops after the atomization process is completed [2], and they have already been included into some CFD models, but there is no general model to predict the initial spray properties for deflecting injectors. As a result, the atomization model is a critical missing link in the modeling of suppressed fires. Moreover, a CFD code with an atomization model will provide a powerful design tool for evaluating the performance of water-based fire suppression systems.

Empirical distributions as well as some other simple correlations which have been developed for estimating characteristic drop sizes based on a few experiments [3-5], can be used as primitive predictive models; however, they have a limited range of validity and are insensitive to many effects that are known to influence the initial spray behavior. The data in these correlations are obtained under quiescent 'cool' conditions. However, the elevated velocities and

temperatures in real fires are expected to influence the atomization process. A robust modeling approach capable of handling this coupling and based on first principles has been used to develop the atomization model in this study. It offers unique insight into the details of the spray by providing initial probability distributions of drop size, velocity, and location. These initial distributions are virtually impossible to obtain experimentally due to the high spray density in the atomization region. Furthermore, FDS 4.0 uses a well established Eulerian-Lagrangian particle tracking method to predict droplet dispersion after atomization, which means the conservation equations for the continuous phase are solved using an Eulerian formulation while the conservation equations for the dispersed phase are solved using a Lagrangian formulation. [33] The spray dispersion can be accurately predicted by using this method when accurate initial conditions are provided. As a result, the atomization model has been integrated into FDS4 in this study, to predict detailed spray characteristics, help design new suppression devices and evaluate the suppression performance in the presence of a real fire. Some important parameters for accurate prediction, such as the number of droplets injected into the computational domain and the resolution of the computational domain will also be discussed in this study.

1.2 Literature Review

1.2.1 Early Sprinkler Measurements

Early experimental work has been conducted to characterize the details of the sprinkler spray. They have utilized photographic techniques [4, 6-9] and a laser-

light shadowing method [5, 10-11]. The photographic methods included illuminating the drops using strobe lighting and pulsed lasers, and using still photographs and video cameras for image capture. The laser-light shadowing technique utilized a modified commercially available instrument intended for cloud drop measurements. The drops were sized by determining the number of pixels shadowed as the drops passed through a visible laser-light sheet illuminating a linear photodiode array. The results from these early experimental investigations provide sprinkler design guidance and provide valuable information for the development of atomization and spray models. Dundas [4] provides drop size measurements for several sprinkler geometries along with a review of drop size data obtained in a variety of injectors. The data is correlated based on an expression first proposed by Heskestad [12] $d_{V50}/D_{orif} = C\,We^{-1/3}$ where d_{V50} is the volumetric median diameter, D_{orif} is the injection orifice diameter, and the Weber number, $We = \rho_l U^2 D_{orif}/\sigma$, is based on the liquid properties. The drop size data compiled by Dundas [4] from various injectors demonstrates that the coefficient of proportionality, *C*, depends on the sprinkler geometry [4]. You's [3] data reveals more insight into the dependency of the coefficient, *C*. His data clearly shows that the *C* increases with increasing injection orifice diameter for upright sprinklers. His spray measurements also show very little change in drop size at different elevations below the sprinkler suggesting that secondary atomization does not occur in sprinkler sprays.

1.2.2 Advanced Sprinkler Measurements

More recently Widmann [13, 14] and Sheppard [5], have characterized velocities and drop sizes from sprinklers using advanced diagnsotics. Widmann used Phase Doppler Interferometry (PDI) to measure drop sizes and velocities from actual sprinklers having *K*-factors ranging from $3.0\ \text{gal min}^{-1}\ \text{psi}^{-1/2}$ ($7.2\times10^{-5}\ \text{m}^3\ \text{s}^{-1}\ \text{kPa}^{-1/2}$) to $5.6\ \text{gal min}^{-1}\ \text{psi}^{-1/2}$ ($1.35\times10^{-4}\ \text{m}^3\ \text{s}^{-1}\ \text{kPa}^{-1/2}$). This measurement technique provides detailed information at one point within the spray, and it involves creating an interference pattern in the region where two laser beams intersect, resulting in a region of alternating light and dark fringes. The region where the laser beams intersect is called probe volume or sample volume. Due to the interference pattern, a droplet passing through the probe volume scatters light exhibiting an angular and temporal intensity distribution which is characteristic of the size, refractive index, and velocity of the droplet. Additional details on the phase Doppler method are available in Ref. 15. Characterizing the overall spray with this technique is prohibitive because of the number of point measurements required to map out the spray distribution. Nevertheless, the drop size and velocity measurements were taken at a number of locations at a given plane to determine the mass flux distribution using the PDI technique. The mass flux obtained from these PDI measurements at specified locations compared favorably with mass flux measurements taken with collection tubes. Widmann also noted deviation from the $p^{-1/3}$ scaling law for droplet size at low pressures (around 69 kPa). Sheppard [5] measured velocities within 200 mm of sprinkler to characterize the initial spray velocity using Particle Image

Velocimetry (PIV). The basic principle of PIV is to illuminate a seeded flow-field with two pulses laser sheet light and record the particle images with a camera. The average displacement of the particles in small regions of the images is calculated using correlation methods. The average velocity in that small region is then calculated by dividing the average displacement by the time between the laser pulses. This technique allows for visualization of a cross-section of the spray [16-18]. He presented these measurements in a spherical coordinate system having the origin located on the sprinkler centerline at a specified position between the orifice and the deflector plate. Sheppard showed the variation of radial velocity with polar angle (measured from the sprinkler centerline) at various azimuthal angles (measured from the sprinkler yoke arms), he also provides a ball-park estimate of the radial velocity close to the sprinkler(~ 0.2 m), which is described by $U_{avg} \approx 0.6\sqrt{p/\rho}$. He compared his velocity measurements with PDI measurements noting discrepancies due to differences in experimental configuration and biasing issues related to the different measurement approaches used in the respective diagnostic techniques. Unfortunately, the PIV technique doesn't provide information on the droplet size distribution or size-velocity correlations, Sheppard used PDI technology to characterize the droplet size distribution for a set of commercial available sprinklers. The results of his analysis confirm the relationship between the volume median diameter and the Weber number postulated by Dunda, however, the proportionality constant appears to be a function of the sprinkler design and the location in the spray.

1.2.3 Atomization Modeling

Predicting spray characteristics has proven to be challenging because of the complexity and stochastic behavior of the breakup process. Theoretical research for investigating liquid jet breakup and disintegration has focused on three general modeling approaches.

The first approach is the surface stability analysis based on wave dispersion theory. In surface stability analysis, the dispersion equations are formulated in terms of a dimensionless wave growth rate and the associated wavelength for specific conditions [19-22]. This approach yields useful information for simple configurations. Dombrowski [23] developed an actual atomization model for fan type injectors based on wave dispersion theory to predict drop size. He described the atomization process in terms of the growth of waves on an unstable sheet. He simplified the wave dispersion equations and integrated them to quantify the sheet breakup characteristics and then related the sheet disintegration to initial drop characteristics. This atomization model based on wave dispersion theory has been successfully used by Rizk for various types of fuel injection systems [24].

The second approach is to use numerical solution with free surface dynamics. The numerical solution approach with free surface boundary calculation has been developed to predict the shape and extent of jets before breakup [25]. The full or simplified multidimensional hydrodynamics equations are solved in this approach. Breakup is calculated directly through surface deformation in the hydrodynamic equations or separately by coupling the previously mentioned wave dispersion analysis with continuous liquid phase behavior predicted from the hydrodynamic

equations. A criterion for breakup must be provided in the latter based on a critical characteristic wavelength to determine the extent of the jets [26, 27]. This approach is appropriate for the impinging jet configuration. Marshall and Di Marzo [28] have developed a complete atomization model for water based suppression injectors by integrating a film formation sub-model proposed by Watson [29] with a sheet disintegration sub-model proposed by Dombrowski [23]. Furthermore, these models have been implemented with a stochastic formulation originally proposed by Rizk [24].

The third approach is to use numerical solution with two-phase flow coupling. Numerical modeling of atomization with two-phase flow coupling requires simultaneous solution of both the liquid and gas phases. The most general fully coupled atomization model is found in the volume of fluid (VOF) approach. [30, 31] A single grid is used in this approach to resolve the continuous liquid and gas phase. The phases are distinguished by a VOF variable which gives the liquid volume fraction for each cell. The interface shape must be reconstructed based on the average liquid volume fraction in each cell in order to compute the face fluxes of gas and liquid. Jet breakup has been determined from semi-empirical formulas and directly from surface tension boundary conditions at the interface using this method. Unfortunately, the VOF method requires very fine grids, smaller than the jet size, in order to resolve the jet surface.

The findings and recommendations of the previous authors provide a strong foundation for this study. The simple correlations obtained from the experimental

data can not accurately provide the initial droplet characteristics for the droplet dispersion model, and they could not predict the changes when the ambient condition changes because of the fire. Alternatively, a fully coupled atomization model could predict the changes of the initial droplet characteristics due to the changes of the ambient condition at the expense of computational time. As a result, an atomization model based on free surface boundary layer and wave dispersion theories will be developed in this study to predict the initial characteristics of droplets, and it will be intergrated with a fully coupled droplet dispersion model to predict spray dispersion. In this approach, partial coupling is provided through specification of the gas phase properties to determine the breakup location, droplet sizes through the wave dispersion relationships, and complete two-phase coupling occurs right after the atomization process. This provides a simplified approach for predicting the change in atomization behavior in the presence of fire.

1.3 Research Objectives

The primary goal of this study is to develop a model to quantify spray atomization and dispersion behavior for the design of water based suppression injectors and for evaluating the performance of water based fire suppression systems. It takes three steps to achieve the primary goal. The first is to develop a primary atomization model that represents the spray breakup mechanism to predict initial drop size, drop velocity, and drop breakup location distributions. The second is to integrate the atomization model into the existing CFD models.

FDS4 is used in this study, and the atomization model provides the initial droplet characteristics for the droplet dispersion model used in FDS4. The third objective is to develop a general algorithm to visualize the particle atomization and dispersion process. The results obtained from the post process code can be compared with the full-scale spray tests data directly.

An additional goal of this study is investigate the sensitivity of the atomization process to operating conditions, such as the injection pressure, ambient gas temperature, and nozzle geometries through modeling and analysis. Comparison with available experimental data will provide guidance for model development and validation. Furthermore, the predictions will provide data at conditions that are not easily obtained experimentally.

Chapter 2: Methodology

In fire research, suppression system design, and even fire investigation, it is of interest to explore if and how fires can be suppressed. Developments in CFD modeling have made it possible to simulate the continuous phase behavior of fires with a high degree of fidelity. For the fire suppression analysis, it is also important to predict the dispersed phase behavior. In order to do that, multiple models are needed, these include a nozzle activation model, an atomization model, a dispersion model, a surface cooling model and a vaporization model. Among these models, an atomization model of the spray is crucial, because the atomization model is required to provide initial conditions for the particle tracking models. However, there is currently no general atomization model that can provide initial drop velocity, location and drop size based on the nozzle geometry and the environmental conditions for sprinklers and other deflected jet atomizers used in suppression devices. Furthermore, scaling laws are nonexistent for predicting initial drop velocity and position, and the scaling laws available for predicting drop size only consider the suppressant properties. However, contrary to conventional thinking, atomization theory reveals that the initial drop characteristics of these low and medium pressure deflected jet injectors are significantly influenced by the surrounding air properties. Development of a general atomization model for deflected jet injectors will be the focus of this study, the initial spray characteristics predicted by this model will be sensitive to injector geometry, injection pressure, ambient temperature, and the gas phase and suppressant properties. After spray atomization, a spray dispersion model will

determine the trajectory of the spray, given the initial spray characteristics provided by the atomization model. The atomization model and dispersion model could also be used in reverse for injector design. The dispersion model would be used to determine the initial spray properties required to meet the penetration criterion in a specific fire environment. The atomization model would help to predict the nozzle geometry required to achieve this spray.

In this study, the atomization model development based on first principles is discussed in detail. Parametric analysis is conducted to see how the nozzle geometries and ambient conditions affect the initial spray characteristics. Dispersion dynamics based on the predicted initial spray characteristics are also explored. Atomization model predictions are the inputs for a modified version 4.0 of the Fire Dynamics Simulator (FDS) for prediction of the spray dispersion.

2.1 Atomization Model Formulation

2.1.1 Atomization Physics

A spray is formed by breaking up a volume of liquid into small drops. This process is referred to as atomization. Water based suppression injectors use atomization to facilitate the dispersion of water over a large area to protect commodities not yet involved in the fire. The spray also delivers water to burning materials and decreases the burning rate by reducing heat feedback to the fuel surface. Moreover, atomization greatly increases the surface area of the injected volume of water. In the case of finely atomized water mist sprays, this increase

surface area results in enhanced evaporative cooling of the hot smoke from the fire and displaces air with inert water vapor. These effects result in abatement or even extinguishment of the fire.

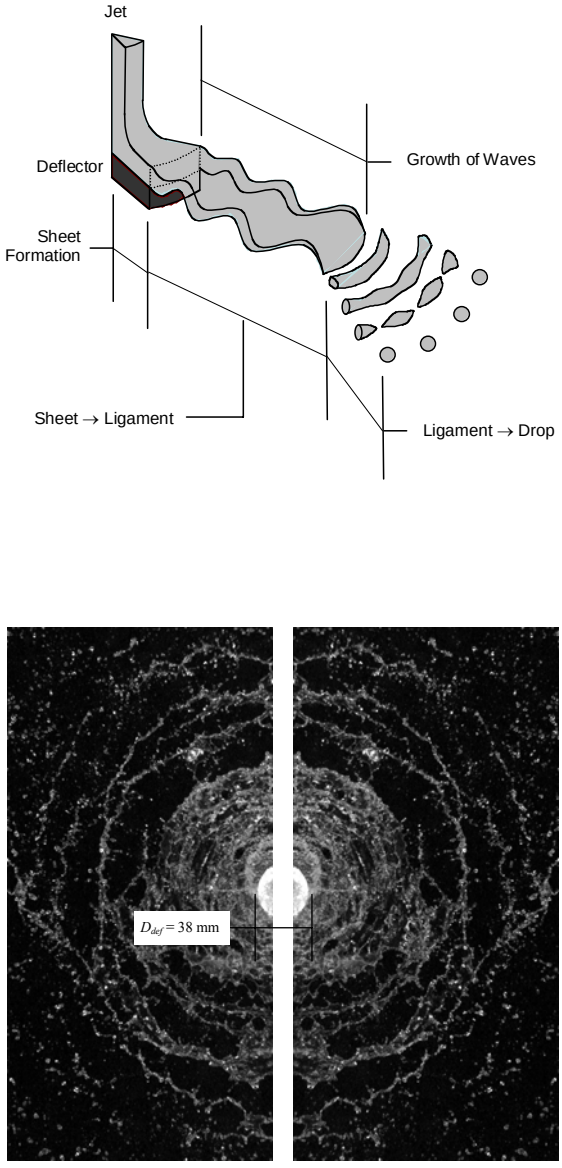

Figure 1.(a) Illustration of the atomization process in conventional sprinklers and low-medium water mist nozzles. *(b)* Grayscale image of the atomization process

For sprinkler and low-medium pressure water mist sprays, the atomization consists of three distinct stages. These stages are clearly illustrated in Figures 1a and 1b. First, the jet formed at the exit of the injection orifice impinges on a striker plate to form a thin film that flows along the plate. This film travels beyond the surface of the plate to form an unconfined expanding sheet. This sheet breaks up more readily than the relatively large-diameter jet formed at the orifice exit. Next, aerodynamic waves are established on the liquid sheet, resulting from the inevitable small disturbances within the flow. These aerodynamic waves are unstable and grow to a critical amplitude which causes the sheet to break into ring-like ligaments. These ligaments are also subject to disturbances and the formation of aerodynamic waves. Finally, the waves on these ligaments grow to a critical amplitude and break the ligaments into small fragments which contract to form spherical droplets. The modeling approach introduced in this paper addresses each stage of the atomization process with physics based sub-models.

2.1.2 Deterministic Model

Sheet Formation

The velocity and thickness of the liquid sheet are critical parameters that govern the atomization process. Because the injection configuration of many water based suppression injectors closely resembles that of an impinging jet, free surface impinging jet theory is used to determine the liquid film thickness and velocity formed on the deflector of a nozzle. The sheet thickness and velocity can easily be determined from these film quantities.

A water jet that impinges on a horizontal plate has been studied by Watson [29] using boundary-layer theory. Watson describes the radial spread of a liquid jet over a horizontal plane by four distinct flow regions. Figure 2 shows these four regions.

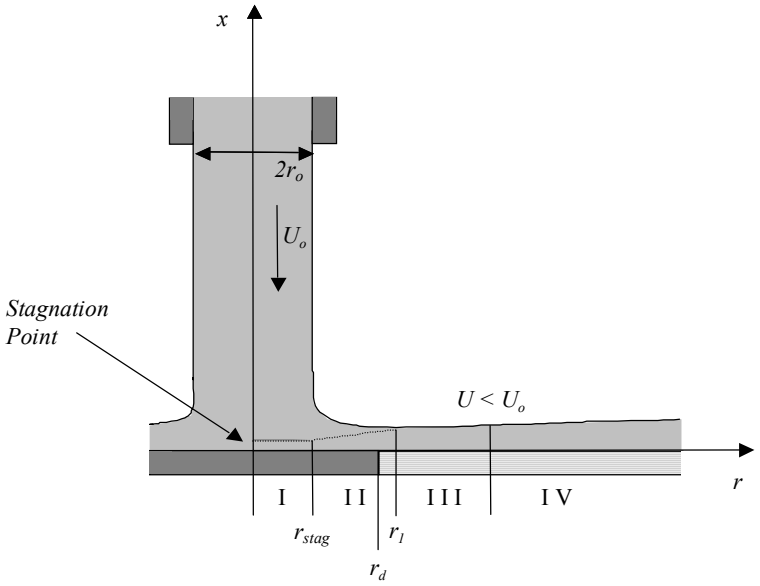

Figure 2. Deflected jet forming a viscous film as it impinges against the deflector. Region specific analytical expressions for the film thickness are available.

Region I: the stagnation region ($r < r_o$, where r_o is the radius of the jet). The speed outside the boundary layer rises rapidly from zero at the stagnation point to U_o, the speed with which the jet strikes the deflector. The effect of the wall is contained in a very thin boundary layer, which is small compared to the film thickness.

Region II: the boundary layer region with Blasius similarity solution ($r < r_1$). The speed outside the boundary layer is unaffected by the layer and remains almost constant and equal to U_o. In this region, the boundary layer grows until the wall influences the entire thickness of the film.

Region III: the transition region. The whole flow is of boundary layer type with velocity profile given by the Blasius solution. The free surface is perturbed by viscous stresses. The velocity profile changes as *r* increases; however, the velocity at the free surface remains nearly equal to U_o.

Region IV: In this region, the speed of the free surface decays more quickly with *r*. Velocity profiles in this region can be described by a non-Blasius similarity solution.

Watson's theory provides region specific expressions for the layer thickness based on the radial location both in laminar flow and turbulent flow. The initial thickness of the sheet is given by the layer thickness at the edge of the deflector. The deflector diameter is thus an important parameter governing the atomization process. Typically, only Region I and Region II have to be considered in sprinkler flow configurations. However, the film has persisted beyond Region II in a few of the high pressure cases studied.

Assuming the motion in the layer is turbulent, for a deflector diameter corresponding to a radial location within Region II where $r_d < r_1$, the sheet thickness is given by

$$h_d = \frac{r_o}{2r_d} + C_1 \times \left(\frac{7\nu_l}{U_o}\right)^{1/5} r_d^{4/5}, \tag{2.1}$$

where r_1 is the radial boundary of region II, r_o is the hydraulic radius of the jet, ν_l is the liquid kinematic viscosity , r_d is the radius of the deflector plate, U_o is the initial speed of the jet, $C_1 = 1.659 \times 10^{-2}$, is a coefficient determined from similarity analysis performed by Watson [29]. It should be noted that this

coefficient will change if the geometry of the nozzle changes (i.e. conical or spherical deflectors). Other coefficients from the similarity analysis are included in subsequent equations and are denoted as C_i.

For deflector diameter corresponding to a radial location beyond region II, the sheet thickness is given by

$$h_d = C_2 \times \left(\frac{\nu_l}{Q}\right)^{1/4} \frac{r_d^{9/4} + l^{9/4}}{r_d}, \tag{2.2}$$

where Q is the mass flow rate of the jet, $C_2 = 0.0211$, l is an arbitrary constant length, which has to be determined by the conditions where the boundary layer reaches the free surface ($r = r_l$). The expression for l is obtained by matching the sheet velocity at $r = r_l$ and is given by

$$l = C_3 \times r_o \left(\frac{Q}{\nu_l r_o}\right)^{1/9}, \tag{2.3}$$

where $C_3 = 4.126$.

The turbulent flow assumption is not always valid over the full range of operating conditions. A stability criterion has been provided by Watson to determine whether the flow is laminar or turbulent. From similarity analysis, Watson derived a criterion jet Reynolds number, $Re = Q/\nu_l r_o = 25{,}700$, above which the flow is turbulent. In the cases presented in the current study, the jet Reynolds number always exceeds this critical jet *Re* for injection pressures above 5 kPa. Therefore, for most cases the region specific expressions for turbulent flow are appropriate for calculating the thickness and velocity of the liquid sheet

at the exit of the deflector. The details of the laminar film formulation can be found in Watson [29].

For a sprinkler or low-medium pressure water mist nozzle, the initial jet size and velocity are easily determined from the injection pressure, nozzle K-factor and liquid desities. U_o can be calculated based on Bernoulli's equation assuming inviscid flow, so that

$$U_o = \left(\frac{2\Delta p}{\rho_l} \right)^{1/2}, \tag{2.4}$$

where Δp is the difference between the total injection pressure and the environmental pressure and ρ_l is the density of the liquid. The hydraulic radius of the jet can be expressed in terms of the nozzle properties by the dimensional equation

$$r_o = \left(\frac{K}{\pi} \right)^{1/2} \left(\frac{\rho_l}{2} \right)^{1/4}, \tag{2.5}$$

where K is the *K*-factor of the nozzle describing the flow characteristics of the injector. The K-factor is typically expressed in units gal min^{-1} $\text{psi}^{-1/2}$ or m^3 s^{-1} $\text{kPa}^{-1/2}$.

The average speed of the sheet when it leaves the deflector plate can be calculated by mass conservation, so that

$$U = \frac{Q}{2\pi r_d h_d} = \frac{K p^{1/2}}{2\pi r_d h_d}. \tag{2.6}$$

Sheet Breakup

The central mechanism for atomization in water based suppression injectors is the breakup of the liquid sheet formed by the injector into ligaments. This process can be observed in Figures 1a and 1b, which shows the sheet breakup process in an impinging jet geometry. This geometry closely resembles that of an injector, however, it should be noted that the impinging geometry does not include the effect of tines which are present in actual nozzles. To describe the liquid sheet breakup process, the wave instability concept is used which assumes that the disintegration of a liquid sheet or a jet occurs when the waves imposed by the surrounding atmosphere reach a critical amplitude. This concept was used by Dombroski [9] to describe the disintegration of viscous liquid sheets. In the model developed in this study, the same concept is used assuming that waves persist and grow on the free surface of the unconfined expanding liquid sheet created by the deflector. The disintegration of the sheet occurs when the wave amplitude reaches a critical value. The sheet breaks forming ring shaped ligaments and drops are produced as the ligaments disintegrate.

In this model, sinusoidal waves are assumed to travel on the surface of the liquid sheet. A force balance is performed on the undulating sheet considering inertial, pressure, viscous and surface tension forces. After considerable reformulation and simplification, the force balance can be expressed in terms of the growth rate of the waves present on the liquid sheet [9]

$$\left(\frac{\partial f}{\partial t}\right)^2 + \frac{\mu_l}{\rho_l} n^2 \left(\frac{\partial f}{\partial t}\right) - \frac{2(\rho_a n U^2 - \sigma n^2)}{\rho_l T} = 0 , \qquad (2.7)$$

where f is the total growth of the wave; σ is the surface tension, n is the wavenumber of the disturbance imposed on the liquid stream ($n = 2\pi / \lambda$), λ is the wavelength, ρ_a is the air density, ρ_l is the liquid density, U is the velocity of the sheet determined previously, T is the thickness of the liquid sheet, t is time, and μ_l is the liquid viscosity.

The speed of the sheet is assumed to be constant and equal to U throughout the breakup process. The change in velocity due to gravitational acceleration has been neglected, because the breakup time is typically less than 10 ms. After the film leaves the deflector plate, the thickness of the sheet decreases continuously as it expands radially. The thickness of the sheet is given by

$$T = \frac{r_d h_d}{r}, \tag{2.8}$$

where T is the thickness of the sheet along its radial extent given by the radial location, r , assuming U = constant.

To simplify the analysis of the atomization process, inviscid fluid is first considered with $\mu_l = 0$, so the Eqn. (2.7) becomes:

$$\left(\frac{\partial f}{\partial t}\right)^2 - \frac{2(\rho_a n U^2 - \sigma n^2)}{\rho_l T} = 0. \tag{2.9}$$

For a specified n, the wave growth rate increases as the sheet velocity increases, which leads to a shorter sheet breakup time. Similarly, decreased air density or increased liquid surface tension results in longer sheet breakup time.

Because the wave with the maximum growth leads to the breakup of the sheet, the corresponding critical wavenumber is of interest. Taking the derivative of

f with respect to n and equating to zero yields the critical wavenumber with the maximum growth:

$$n_{inv,crit} = \frac{\rho_a U^2}{2\sigma} \quad . \tag{2.10}$$

Since the wavelength is inversely proportional to the wavenumber, the critical wavelength which leads to the breakup of the sheet increases as the liquid surface tension increases but decreases as the air density or sheet velocity increases.

After substituting Eqn. (2.10) into Eqn. (2.9), the sheet breakup time can be determined by integrating Eqn. (2.9) with respect to time. Assuming that the sheet velocity U will remain constant until breakup, the breakup radius, r_{sh}, can be determined from calculating the time taken to reach a critical dimensionless amplitude, $f_{crit,sh}$. This critical dimensionless amplitude can be determined experimentally and has been found not to depend on operating conditions, however, it may depend on the general injector configuration [9, 13]. A constant value, $f_{crit,sh} = 12$, applied in this model [9].

Although the inviscid flow assumption simplifies the problem significantly and provides some insight into the governing parameters, it is not realistic. For wave growth on liquid films with finite viscosity, Eqn. (2.7) is solved for $\partial f / \partial t$ which is then integrated to determine the time to reach breakup ($f_{crit,sh} = 12$). Critical breakup times are determined over a range of wavenumbers. The breakup time is minimized with respect to wavenumber and the wavenumber, $n_{crit,sh}$, corresponding to this minimum, $t_{bu,sh}$, is the most unstable wave leading to sheet breakup.

The sheet is assumed to breakup into ring-like ligaments having an inner radius equal to the breakup radius, $r_{bu,sh} = r_d + Ut_{bu,sh}$, a radial width given by $\lambda_{crit,sh}/2$, and a thickness given by the sheet thickness at breakup, $h_{bu,sh}$. The mass of the ligament, m_{lig}, is thus given by

$$m_{lig} = \pi\rho_l h_{bu,sh}[(r_{bu,sh} + \pi / n_{crit,sh})^2 - r^2{}_{bu,sh}] \ . \tag{2.11}$$

An equivalent diameter, d_{lig}, for the ligament can be determined from

$$m_{lig} = \pi^2 \rho_l \frac{d_{lig}^2}{2}\left(r_{bu,sh} + \frac{d_{lig}}{2}\right) \ . \tag{2.12}$$

The goal of the sheet breakup analysis is to find the critical wave number with maximum growth which causes the sheet breakup. The ligament diameter can then be obtained from the mass of the sheet fragment after breakup. The ligament diameter is governed by the critical sheet breakup wavelength, sheet thickness at breakup, and the sheet breakup location. The ligament diameter is most sensitive to the change of the critical sheet breakup wavelength, and it increases as the critical sheet wavelength increases.

Ligament Breakup

The ligaments formed from the sheet breakup are also unstable and subject to the growth of waves that lead to ligament fragmentation into drops. Weber [39] has analyzed the properties of these waves where surface tension forces predominate, the critical ligament breakup wave number could be calculated by Eqn. (2.13):

$$nd_{lig} = \left[\frac{1}{2} + \frac{3\mu_l}{2(\rho_l \sigma d_{lig})^{1/2}} \right]^{1/2} \tag{2.13}$$

For the sprinkler spray breakup, the second term in the square brackets in Eqn. (2.13) is negligible, but for a water mist system, since the ligament diameter will be relatively small, the second term in the square brackets becomes more important. The effect has been included in the code. Assuming fragment with the length of the critical ligament break up wavelength will contract into a droplet. Conserving the mass on the fragment, the characteristic droplet diameter, d_{drop}, is

$$d_{drop} = d_{lig}^{2/3} \left(\frac{3\lambda_{crit,lig}}{2} \right)^{1/3} . \tag{2.14}$$

The number of drops that are formed after ligament breakup can be expressed as

$$N = \frac{6m_{lig}}{\rho_l \pi d_{drop}^3}, \tag{2.15}$$

determined by conserving mass between the ligament and the drops.

Weber [39] also provides an expression for the breakup time as

$$t_{bu,lig} = 24 \left(\frac{2\rho_l}{\sigma} \right)^{1/2} \left(\frac{d_{lig}}{2} \right)^{3/2} . \tag{2.16}$$

The distance that it takes for the ligaments to disintegrate into drops is easily calculated from the ligament velocity, U, and $t_{bu,lig}$. The initial drop location, which is the total distance the liquid travels until drops are formed, is given by

$$r_{drop} = r_d + U(t_{bu,sh} + t_{bu,lig}) . \tag{2.17}$$

The initial spray velocity, U, initial spray drop size, d_{drop}, and initial spray location, r_{drop}, are completely defined by Eqns. (2.6), (2.14), and (2.16), respectively. These quantities are determined from the nozzle geometry (K, r_d),

injection pressure (p), surrounding flow gas phase conditions (ρ_a, μ_a), and liquid properties (σ, ρ_l, μ_l). It should be noted that for the current formulation, the velocity of the gas in the vicinity of the sheet was assumed to be zero; however, the velocity of the fire and even the spray induced flow would change the relative velocity of the sheet. This relative velocity could replace the sheet velocity in Eqn. (2.6). These atomization relationships provide characteristic initial spray conditions for a given nozzle geometry and injection pressure, fire condition, and liquid suppressant. Of course in real applications, a multitude of drops with different sizes are created. In order to model this behavior a stochastic analysis [10] is introduced.

2.1.3 Stochastic Model

In the stochastic atomization formulation, random behavior with a physical basis is added into the drop formation model to obtain the distributed drop characteristics. This physics based technique provides an alternative to specifying a standard distribution about a calculated characteristic drop size. The liquid film velocity, the liquid sheet to ligament breakup wavelength, and the ligament to droplet breakup wavelength are treated stochastically. The stochastic model ultimately provides distributions for initial drop size, velocity, and location.

In the deterministic model, the liquid sheet velocity is assumed to be constant during the breakup process. In the stochastic model, a distribution for the liquid

sheet velocity is introduced through a turbulence intensity. This turbulence intensity is defined as

$$I_u = \frac{\sqrt{\overline{u'^2}}}{\bar{U}}, \tag{2.18}$$

where the velocity magnitude is given by $\bar{U} + u'$, $\bar{U}$ is the mean velocity magnitude, and u' is the fluctuation zero-mean velocity magnitude. Assuming that the liquid sheet velocity has a Gaussian probability density distribution, the stochastic model generates a set of random sheet velocities, $U_i = \bar{U} + u_i'$, which satisfies the Gaussian distribution based on the given turbulence intensity and the value of the mean liquid sheet velocity. The mean liquid sheet velocity is determined from the injection pressure and sheet formation model. The subscript *i* counts the *m* specified number of random velocities. The distribution of liquid sheet velocities is used in the wave dispersion model resulting in different critical sheet breakup wavelengths, sheet breakup times, and sheet breakup locations. These distributed parameters will influence the subsequent ligament formation and breakup analysis.

In the sheet breakup model, the sheet is assumed to breakup into ring-like structures having radial width of one-half wavelength. These ring-like structures rapidly contract into torroidal ligaments, which in turn break up into drops. The sheet, of course, does not always breakup into one-half wavelength sections. In the stochastic model, a set of random characteristic sheet fragment lengths, $(l_{bu,sh})_{i,j}$, are generated to describe the uncertainty of sheet breakup based on the

mean sheet fragment length, $(\overline{l_{bu,sh}})_i$, which equals to half of the critical sheet breakup wavelength, $(\lambda_{bu,sh})_i$, and sheet breakup turbulence intensity. The subscript *j* counts *n* possible sheet breakup lengths for each character sheet breakup length $(\overline{l_{bu,sh}})_i$. The shape of the characteristic sheet fragment length distribution for each of the *i* different sheet breakup realization of events associated with the velocity distribution is determined using a normalized Chi-Square distribution. These fragment length distributions are determined from the sheet breakup turbulence intensity, I_{sh}. In the Chi-Square distribution, the standard deviation, σ_{cs}, is depending on the mean value of the Chi-Square distribution, μ_{CS}, the turbulence intensity for Chi-Square distribution is given by

$$I_{CS} = \frac{\sigma_{CS}}{\mu_{CS}} = \frac{\sqrt{2\mu_{CS}}}{\mu_{CS}} = \sqrt{\frac{2}{\mu_{CS}}} \quad , \tag{2.19}$$

where $\mu_{CS} \geq 2$. The shape of the Chi-Square distribution is completely determined by μ_{CS} which can be expressed in terms of I_{CS}. The turbulence intensity specified for the sheet fragments is given by

$$I_{sh} = \frac{(\overline{l'_{bu,sh}})_i}{(\overline{l_{bu,sh}})_i}, \tag{2.20}$$

where $(\overline{l'_{bu,sh}})_i$ is the standard deviation of the sheet fragment lengths, which cannot exceed the mean sheet fragment length $(\overline{l_{bu,sh}})_i$ for the Chi-Square distribution, which is half of the critical sheet breakup wavelength $(\lambda_{bu,sh})_i$. It is used to generate a discrete Chi-Square Distribution so that

$$\mu_{CS} = \frac{2}{(I_{sh})^2}, \tag{2.21}$$

Where $0 < I_{sh} < 1$. The quantity μ_{CS} completely specifies the Chi-Square Distribution [34]. This distribution is normalized by μ_{CS} and multiplied by the mean sheet fragment length $(\overline{l_{bu,sh}})_i$ to create *m* Chi-Square sheet fragment length distributions each having *n* different lengths specified by $(l_{bu,sh})_{i,j}$. The specified turbulence intensity I_{sh} is maintained when converting the Chi-Squiare distribution to the sheet fragment length coordinate. Figure 3 shows the normalized Chi-Square distribution shape with different turbulence intensities:

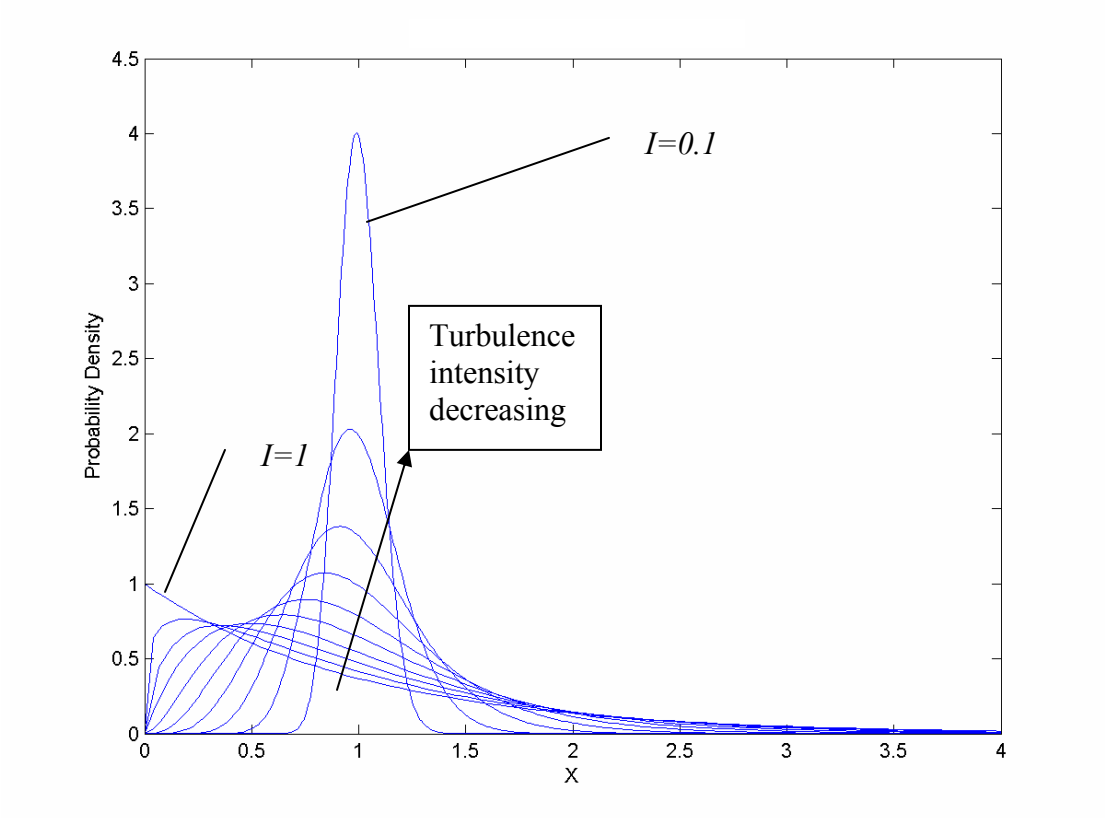

Figure 3. Normalized Chi-Square distribution

The Chi-Square distribution provides a physically realizable distribution of possible sheet breakup lengths and prevents the occurrence of negative breakup lengths at high turbulence intensities.

In the ligament breakup model, the torroidal ligament is assumed to breakup into fragments having a length of one critical ligament breakup wavelength. Each fragment contracts into one drop. It is not always the case that the ligament breaks up into a fragment with a length of one critical ligament breakup wavelength, so in the stochastic model, a set of random ligament fragment lengths are generated to describe the uncertainty of ligament breakup based on a mean ligament fragment length which equals to the critical ligament breakup wavelength, and ligament breakup turbulence intensity. Similar to the sheet breakup analysis, the shape of the ligament fragment length distribution is determined using a normalized Chi-Square distribution based on the ligament breakup turbulence intensity, I_{lig}, which is expressed as

$$I_{lig} = \frac{(\overline{l'_{bu,lig}})_{i,j}}{(\overline{l_{bu,lig}})_{i,j}}, \tag{2.22}$$

where $(\overline{l'_{bu,lig}})_{i,j}$ is the standard deviation of the ligament fragment length, which cannot exceed the mean ligament fragment length $(\overline{l_{bu,lig}})_{i,j}$ for the Chi-Square distribution. $(\overline{l_{bu,lig}})_{i,j}$ equals to the critical ligament breakup wavelength $(\lambda_{bu,lig})_{i,j}$. Recall from the ligament breakup analysis, the critical ligament fragment wavelength, $(\lambda_{bu,lig})_{i,j}$, is determined by the mean sheet fragment length $(l_{bu,sh})_{i,j}$. The ligament fragment lengths are determined from a set of $m \times n \times p$

random ligament breakup lengths $(l_{bu,lig})_{i,j,k}$, where *k* counts *p* possible ligament fragment wavelengths for each mean ligament fragment length $(\overline{l_{bu,lig}})_{i,j}$, corresponding to each critical ligament breakup wavelength $(\overline{\lambda_{bu,lig}})_{i,j}$. As a result, a set of $m \times n \times p$ possible drop sizes $(d_{drop})_{i,j,k}$ are determined in the stochastic model. The number of drops having the same drop size can also be obtained by conserving the mass between the ligament and the drops. The number of drops is determined assuming each ligament forms an equal number of drops from each of the *p* possible drop sizes.

The introduction of stochastic behavior in this three stage droplet formation model yields initial drop size, drop velocity, and drop location distributions. The stochastic formation is summarized in the following. In the stochastic model, *m* liquid sheet velocities, U_i, are generated, which result in *m* different critical sheet breakup wavelengths, $(\lambda_{bu,sh})_i$, corresponding to *m* different mean sheet fragment lengths, $(\overline{l_{bu,sh}})_i$. For each mean sheet fragment length, *n* sheet fragment lengths, $(l_{bu,sh})_{i,j}$, are generated, resulting in $m \times n$ sheet fragment lengths, which lead to $m \times n$ critical ligament breakup wavelengths, $(\lambda_{bu,lig})_{i,j}$, corresponding to $m \times n$ mean ligament fragment lengths, $(\overline{l_{bu,lig}})_{i,j}$. For each mean ligament fragment length, *p* ligament fragment lengths, $(l_{bu,lig})_{i,j,k}$, are generated, which result in *p* different droplet diameters, $(d_{drop})_{i,j,k}$. In all, $m \times n \times p$ possible drop sizes are obtained in the stochastic model together with the number of drops at each of the possible drop sizes. In the current study, *m*, *n*, and *p* are specified as

1000, 50, 50, respectively in order to obtain sufficient statistics for a smooth drop size distribution.

2.2 FDS Modification

2.2.1 Overview of FDS Sprinkler Model

FDS 4.0 has a comprehensive sprinkler model for predicting sprinkler activation, spray dispersion as well as the interaction between the spray and the fire. It includes multiple sub-models: a sprinkler activation model, a spray specification model, a droplet tracking model, a droplet vaporization model, a surface cooling model, and a model to predict the interaction between the droplets and fire. The atomization model and dispersion model are the focus of this study.

In the FDS 4.0 sprinkler model, the information for a specific nozzle should be provided in the sprinkler file (.spk file) by the user. The information includes the sprinkler activation parameters, the initial spray properties as well as the normal operating condition of the nozzle. Table 1 includes the typical input variables that are specified in the ".spk" file, more information could be found in Ref. [36]. It can be seen that most of the information provided in the sprinkler file is used to specify the initial spray, including the initial drop size, drop location and the drop velocity. In the FDS sprinkler specification model, the initial droplet size distribution of the sprinkler spray is expressed in terms of its Cumulative Volume Fraction(CVF), a function that relates the fraction of water volume transported by droplet less than a given diameter. A combination of log-normal

Table 1. Nozzle Specifications in FDS Sprinkler File

Variable Names Use in FDS	Definition
K-FACTOR (L/min/bar$^{1/2}$)	K-Factor of the nozzle, represents the D_{orif} of the nozzle
ACTIVATION_TEMPERATURE (^{o}C)	Link activation temperature
OPERATING_PRESSURE (bar)	The pressure at which the nozzle was tested
OFFSET_DISTANCE (m)	Initial droplet location
VELOCITY	Description of the initial droplet velocity distribution, including specification of average velocity, V_{mean}, maximum spray angle θ_{max} and minimum spray angle, θ_{min}.
SIZE_DISTRIBUTION	Information about the initial droplet distribution, including the specification of d_{V50}, and the coefficients used in the Cumulative Volume Fraction correlation, γ and σ.

and Rosin-Rammler distributions suggested by the researchers at Factory Mutual is used in the FDS spray specification model:

$$F(d) = \begin{cases} \dfrac{1}{\sqrt{2\pi}} \displaystyle\int_0^d \frac{1}{\sigma_d'} e^{-\frac{[\ln(d'/d_{V50})]^2}{2\sigma^2}} dd' & (d \le d_{V50}) \\ 1 - e^{-0.693\left(\frac{d}{d_{V50}}\right)^{\gamma}} & (d_{V50} < d) \end{cases} \tag{2.23}$$

The d_{V50} and the empirical constants γ, σ, are specified in the sprinkler file. These values are determined by testing the sprinkler in a cool quiescent environment. The size of a given droplet is randomly chosen based on the distribution described in Eqn. (2.24). The mean velocity of the initial droplet is specified in the sprinkler file assuming that the nozzle is running at the operating pressure. FDS users can desire to flow the nozzle at a different pressure other than the operating pressure, using command "PIPE PRESSURE" in the input file. Since the velocity of the droplet, V, is proportional to $\sqrt{p}$, FDS will calculate the initial droplet

velocity by $V_{ini} = V_{mean} \times \sqrt{P_{pipe} / P_{operating}}$. Moreover, the initial spray in FDS is assumed to be a symmetric hollow cone shape spray, so the minimum and maximum spray angle, θ_{min} *and* θ_{max} should be specified in the sprinkler model. For a given droplet, the direction of the droplet velocity is determined by randomly choosing an elevation angle, θ, from θ_{min} to θ_{max}, and randomly

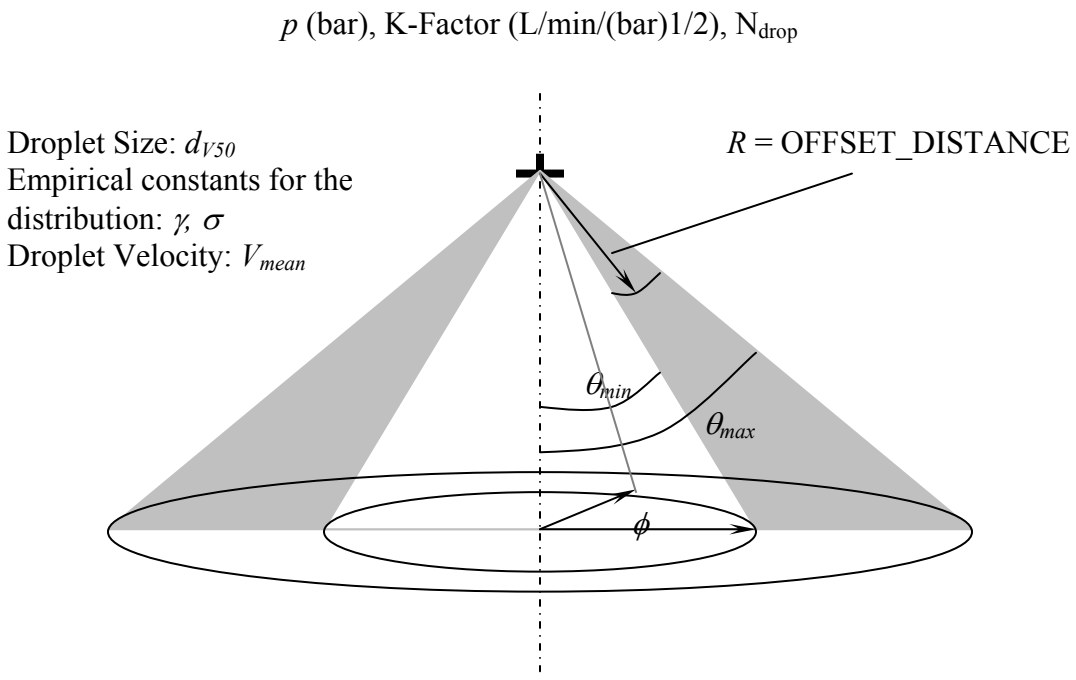

Figure 4. Input parameters for spray specification

choosing an azimuthal angle, Φ, range from 0 to 2π. The initial location of the droplet is determined by the "OFFSET_DISTANCE" specified in the sprinkler file by the user and the randomly chosen θ *and* Φ. The "OFFSET_DISTANCE" is the distance from the sprinkler orifice where water droplets are initialized. Actually, there is another way to specify the initial droplet size and droplet

velocity in FDS model instead of giving a mean median volume diameter and mean velocity for the entire spray, the median droplet size and the velocity could be given as a function of the azimuthal angle. However, more tests are needed to get the spray information in such details. In addition to the previously described input variables, the number of droplets inserted into the computational domain per second is specified in the input file, this value will determine how many droplets will be tracked in the particle tracking model. The larger the number is, the more computational time is needed, but the better the whole spray will be represented. The input parameters for the sprinkler specification model discussed above are shown in Figure 4.

After the water droplets are initialized, the particle tracking model is used. The FDS dispersion model uses a complete two-phase coupling, Eulerian-Lagrangian particle tracking method. The gas phase behavior is calculated within each cell every time step, the trajectory of the droplet in the air is calculated by solving the governing equation in a Lagrangian form using the updated gas phase information. A droplet vaporization model and transportation model are also included in the FDS dispersion model. One thing should be noted is that not every droplet of the spray is tracked in the dispersion model, only a set of droplets (N_{drop}) is tracked, these droplets are considered to be representative drops that carry the mass for the whole spray. As a result, a weighting factor is calculated from conserving the mass of the spray:

$$\dot{m}\delta t = C\sum_{i=1}^{N_{drop}} \frac{1}{6}\pi\rho_l d_i^3 \tag{2.24}$$

where $\dot{m}$ is the mass flow rate of the water leaving the nozzle, C is the weighting factor. This weighting factor is used in the transport model [33].

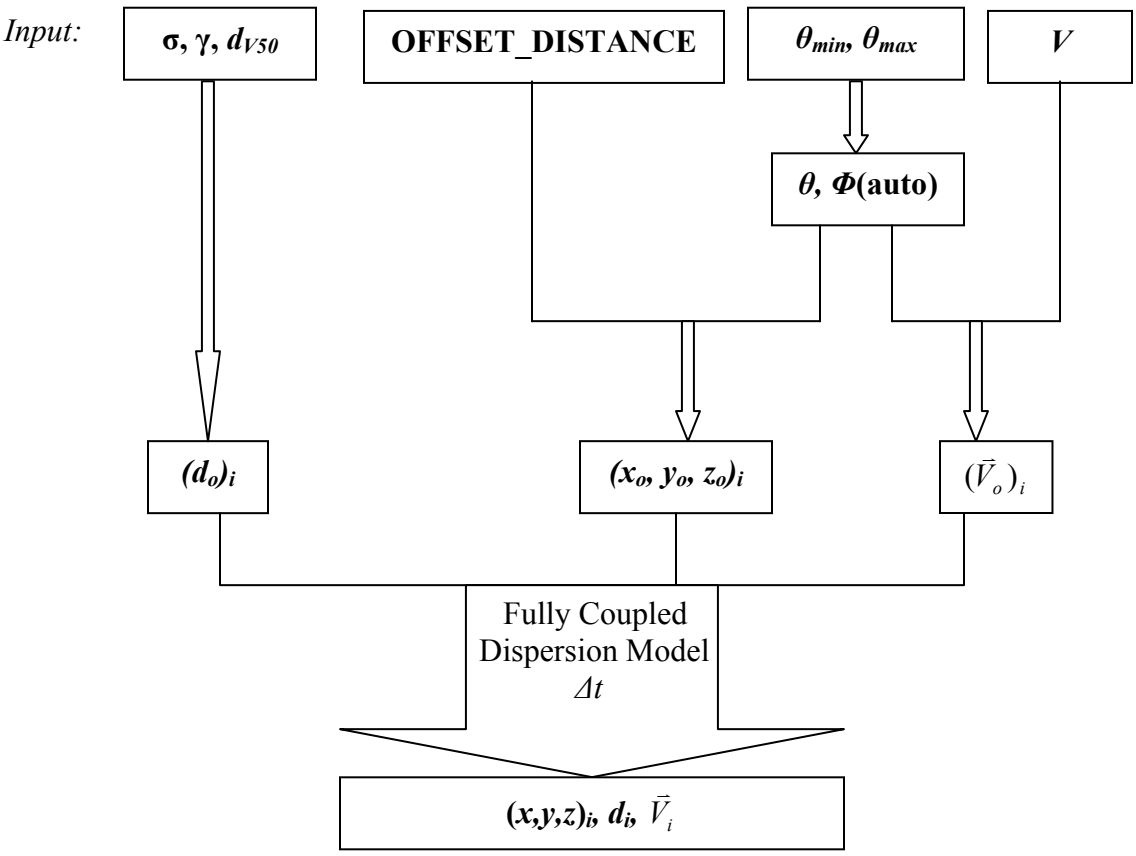

Figure 5. Flow Chart of FDS spray specification and dispersion model

Take one droplet for example, the entire procedure of droplet specification and spray dispersion calculation in FDS is shown in Figure 5. All the input parameters are obtained from the sprinkler tests in a quiescent environment or user experience and the initial droplet size, droplet velocity, and droplet location are specified independently. However, the theory predicts that the initial spray properties will change because of the elevated temperature caused by the fire, and the initial droplet location and the initial drop velocity should depend on the

droplet size, which will be demonstrated later in the next chapter. In the following, the atomization model presented before will be integrated into FDS sprinkler model to specify the initial spray.

2.2.2 Integrating the Atomization Model into FDS

The FDS spray specification model takes the initial droplet size distribution as a combination of Rosin-Rammler and log-normal distributions, which may not accurately represent a real sprinkler spray. The initial droplet size, velocity and location specifications are based on spray dispersion tests. The spray characteristics obtained in these tests may not be suitable in real fire scenarios because of the potential strong coupling between the fire and the spray. Moreover, the relationship between the droplet size, drop velocity and initial drop location doesn't appear in the FDS spray specification model. As a result, an atomization model has been partially integrated with FDS as a first step in addressing the deficiency.

There are several ways to integrate the atomization model into FDS. The easiest way is to curve fit the droplet size distribution predicted by the stochastic atomization model using the combination of Rosin-Rammler and log-normal distribution, and to use the predicted characteristic droplet size, droplet velocity and the drop location to specify the initial spray characteristics in the sprinkler file. So that, the effect of the fire on the initial spray characteristics is accounted for, and there would be no need to perform spray dispersion tests. However, the drop size, drop location and the drop velocity would be specified independently, and an

empirical distribution would still be required using this method. Since the FDS code is organized into several modules, the best way to integrate the atomization model is to incorporate the atomization model as a sub-model of FDS, and to call the atomization model subroutine or atomization module to calculate the initial spray characteristics. In order to build the atomization module, many things, such as the FDS input data file, the sprinkler file name list, the read module etc. would need to be changed. As a result, we compromised in this preliminary attempt to couple the atomization model with FDS. The output file of the initial droplet size distribution, and the corresponding average initial drop velocity and drop location predicted by the stochastic atomization model are used as inputs for the FDS code to specify the initial spray. The subroutine in FDS for the initial spray specification was replaced by a new subroutine, which randomly chooses the droplet size from the droplet size distribution predicted by the atomization model. The procedure for selecting droplet sizes is as follows: choose N_{drop} uniformly distributed random numbers between 0 and 1, which correspond to N_{drop} values of Cumulative Number Fraction (converted from the cumulative volume fraction) and obtain N_{drop} droplet diameters based on the Cumulative Number Fraction values. Once the droplet diameter is selected, the corresponding average initial droplet velocity and the droplet location predicted by the atomization model are assigned to that droplet. Since the relationship between the initial drop size with the initial droplet velocity and the initial droplet location has been accounted for in the atomization model, the modified FDS code accounts for the relationship as well. For instance, the results predicted by the atomization model show that small

droplets tend to breakup closer to the centerline of the sprinkler, and have bigger velocities. So by using the modified FDS model, the smaller droplets will have larger initial velocities and the initial locations of the smaller droplets will be closer to the center of the nozzle. The spray angles are not specified using the atomization model, the initial droplets are assumed to travel horizontally (θ=0), the azimuthal angle, Φ, is randomly chosen from 0 to 2π. The initial spray specification procedure is shown in Figure 6:

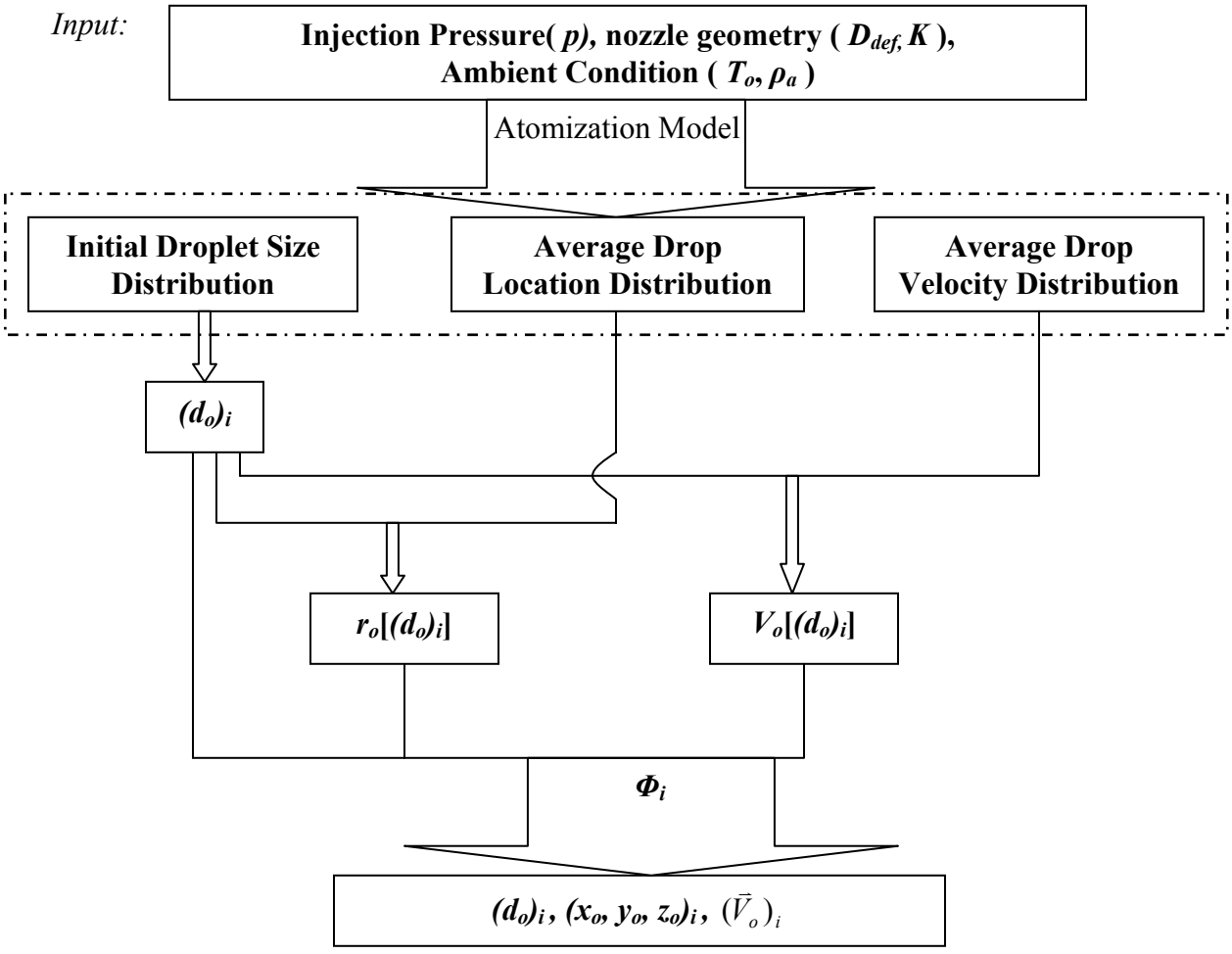

Figure 6. Specification procedure of initial spray using atomization model

After the spray is initialized, the initial spray characteristics will be used as the input for the spray dispersion model to predict the spray dispersion behavior.

2.2.3 FDS Spray Post-Processing

The original FDS code provides detailed gas-phase information within the computational domain in an Eulerian form, it could also provide droplet trajectories after atomization. However, the dispersed-phase information in Eulerian form is more often needed. For instance, in sprinkler tests, the SMD is measured for a long period at specific locations, in order to compare the predicted SMD with the experimental data, droplet size information at that point is needed; or if the droplet water mass flux distribution in a given plane is to be characterized, the Eulerian information is needed. Moreover, the original FDS code can only provide the diameter of the droplet, the temperature of the droplet, and the velocity magnitude of the droplet. As a result, a spray post processing algorithm was developed in this study.

The computational domain in FDS is divided into $NX \times NY \times NZ$ cells, and at a certain time step, the locations of the droplets are calculated in FDS. First, the droplet location is transferred into a position vector to indicate which cell the droplet is in for all the droplets in the computational domain at that time step. Second, the droplet information is averaged by mass within each cell, to get the average droplet properties at a certain location at an instantaneous time. The droplet properties include the Sauter Mean Diameter (SMD), temperature, droplet velocity magnitude as well as velocity components in three directions, and water

mass flux in three directions. The drops are treated differently from the continuous gas phase. In the continuous phase, spatial-averaging is performed within the eight adjacent cells. However, the previously described methodology calculated the actual value of the average droplet properties in each cell. These values are written into a droplet plot3D file and all these modifications have been done within the FDS source code. All the droplet properties are output to the droplet plot3D at one instantaneous time at a certain time interval, another time-averaging algorithm will be used to deal with the time averaging of the droplet properties within a given time period. A frequency factor which represents how often droplets reach a given location is calculated besides all the droplet properties by this time averaging program.

In addition, the droplet information for a given droplet will not be provided until the next time step after the injection of that droplet in FDS, as a result, the initial droplet information could not be seen by the origin FDS code. Small modifications have also been made into the FDS code in this study to visualize the initial spray.

2.3 Model Limitations

The atomization model developed in this study based on first principles is the first step to address the deficiency of the current initial spray specification models used in most current CFD models. But there are still limitations about this simple atomization model.

First, the atomization model in this study is developed based on a simple geometry. The spray formation process is simplified as an impinging jet impinges onto a horizontal plate. However, the shape of most deflectors is much more complicated than a horizontal plate. There are cone shape deflectors, spherical deflectors, plate deflectors with tines and some other special shapes combining all these basic shapes. For different deflectors, the equations which determine the sheet thickness and velocity will be different. For example, if considering the tines effect on a plate deflector, the velocity direction of the droplet will change, the spray will become less hollow. Currently, we have derived formulas to calculate the sheet thickness and velocity for simple conical and spherical deflectors, and an atomization model for a more complex sprinkler configuration should be developed in the future.

Second, in the atomization model, the dispersed phase and the gas phase behavior has not yet been fully coupled. The gas properties do appear in the governing equation for the liquid breakup, however, liquid behavior doesn't influence the momentum or composition of the gas in the model, and the sheet orientation is not affected by gas. Furthermore, the relative velocity is specified assuming quiescent ambient gas. The gas velocity in the atomization region changes with time and space. The relative velocity based on the gas velocity should be considered. The complete two phase coupling doesn't occur until the drop dispersion stage.

Third, in the atomization model developed in this study, only the wave instability breakup mechanism has been considered. Other breakup mechanisms

are also possible, such as the boundary-layer stripping breakup mechanism. As a result, the droplet size distribution may be different from the real spray droplet size distribution. Other possible primary breakup mechanisms will be added into the atomization model in the future for better predictions of the droplet size distribution.

Fourth, in the stochastic atomization model, the turbulent intensities for sheet velocity, sheet breakup and ligament breakup are the input parameters. These parameters are expected to be influenced by the injector geometry and injection pressure. Currently these values can only be estimated until data or models are available to provide guidance on values for these parameters. Careful measurements of these values are currently being conducted to support continued development of the atomization model. However, the predictions show great agreement with the experimental data using these parameters in a certain range.

Fifth, only preliminary coupling has been developed between the atomization model and the FDS code. The atomization model has not been included into FDS as a sub-model. The gas properties will change with time, so the initial droplet characteristics should change with time as well. However, the initial droplet characteristics are calculated using the gas properties specified in the atomization model, which doesn't change with time. In addition, if the atomization model has been fully coupled with FDS, the number of droplets will be calculated automatically instead of specifying in the input. In addition, the FDS spray-post processing code is only valid for uniform grids.

Chapter 3: Results and Discussion

3.1 Overview

The atomization model developed in this study is a pseudo-coupled atomization model, which means that the initial gas phase temperature and velocities are assumed and input into the atomization model for predictions of initial drop properties. But in a fully coupled model, the calculated gas phase properties in the atomization region and the relative velocity of the sheet would be continuously updated for recalculation of the transient spray development. Nevertheless, the atomization model developed in this study still reveals more interesting insight into the spray behavior; it can provide overall statistical quantities of the spray and it is able to provide inputs for CFD models. By combining the atomization model and the particle tracking capabilities of CFD, distributed spray quantities and dispersion behavior can be studied.

The atomization model is evaluated from several perspectives in this study to determine its suitability and potential for fire suppression applications. The predicted droplet size distributions are compared with the UMD's experimental data using an ideal lab deflected jet atomizer. The median volume droplet size and the droplet size distribution obtained from the stochastic model will be compared with correlations and the experimental results obtained by other researchers as well. The atomization model will also reveal insight to details of spray dynamics which have not been previously considered for fire suppression. For instance, the geometry of the sprinkler, the ambient operating condition and the liquid

properties will change the initial droplet characteristics which will in turn change the droplet dispersion.

3.2 Deterministic Analysis

The deterministic atomization model is useful for predicting characteristic initial droplet size, droplet velocity, and the droplet location and it can be used to evaluate the sensitivity of a spray to changes in fluid properties, nozzle geometries, injection pressures and ambient temperatures.

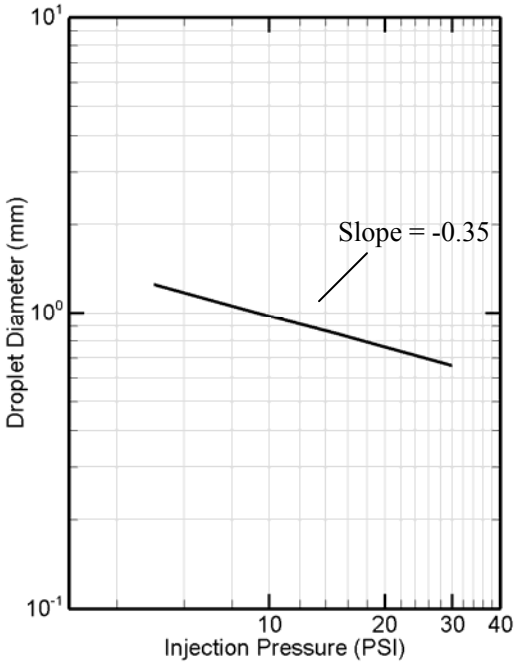

Figure 7. Predicted relationship between the characteristic droplet sizes and the injection pressures of spray at standard atmospheric condition, K = 3 gal min^{-1} $psi^{-1/2}$, D_{def} = 38 mm

Figure 7 shows the predicted relationship between the initial characteristic droplet size and the injection pressure. The K-factor of the nozzle is 3.0 gal min-

[1]psi $^{-1/2}$, and the diameter of the deflector, D_{def} is 38 mm, the injection pressure varies from 5 to 30

psi. The results predicted by the deterministic model show that the characteristic droplet size is proportional to $p^{-0.35}$ which is consistent with the Heskestad's $p^{-1/3}$ scaling law [12] for droplet size.

To evaluate the sensitivity of the spray to the changes of ambient temperature and injection pressure, Figure 8 shows the initial drop size and location as a function of ambient temperature and injection pressure for the same nozzle having K = 3 gal min^{-1} psi $^{-1/2}$, D_{def} = 38 mm. These modeling results demonstrate the strong coupling between the ambient temperature and the atomization process.

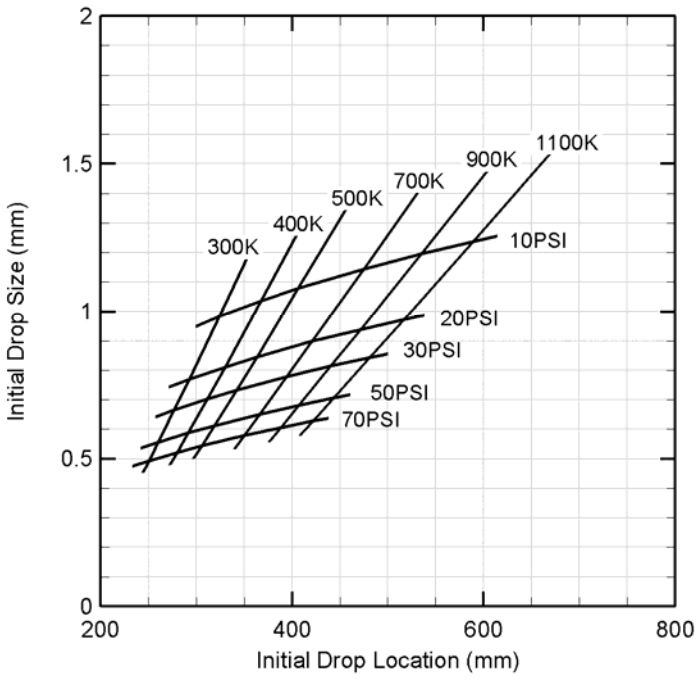

Figure 8. Predicted initial drop conditions of a sprinkler spray as a function of injection pressure and ambient temperature, K = 3 gal min^{-1} psi $^{-1/2}$, D_{def} = 38 mm

The model suggests that the initial spray at the time of sprinkler activation and at various stages of the fire will differ from those measured under room temperature conditions. It should be noted that the typical activation temperature, 300 K-350 K, corresponds to the sensor temperature and the smoke layer may be at a much higher temperature at the time of activation. As the ambient temperature increases, the drop size increases and the breakup length increases. Although these modeling results were obtained with the full deterministic viscous model, the simpler inviscid wave growth equations can be used to explain this behavior. Combining Eqns. (2.9) and (2.10) reveals that the wave growth rate varies linearly with ambient density. Increases in the ambient temperature result in lower ambient densities, slower wave growth rates and corresponding longer breakup distances. Evaluation of Eqns. (2.9) – (2.14) demonstrates that the droplet diameter is a weak function of the ambient density and corresponding ambient temperature. Figure 8 also illustrates the effect of injection pressure on the spray. The drop size and breakup length are both significantly reduced by increases in injection pressure for a specified ambient temperature.

Changes in sprinkler geometry will also affect the initial spray characteristics significantly. Figure 9 shows the effects of changing K-factor, which is a measure of the effective sprinkler orifice size, and the effects of changing the deflector diameter. The drop size and breakup length are significantly increased with increasing *K*-factor. Figure 9 also shows that the drop size and breakup length are

relatively insensitive to changes in the deflector diameter. Initial drop sizes are shown for deflector diameters ranging from 25 mm to 51 mm for each *K*-factor.

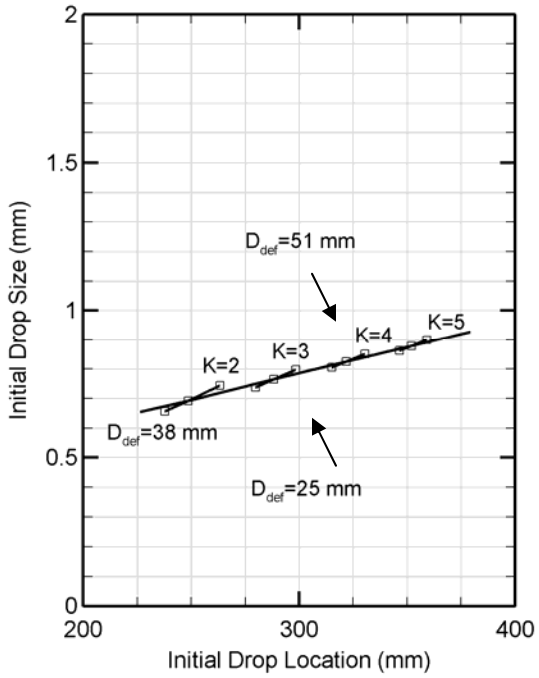

Figure 9. Drop size and initial drop location predictions of a sprinkler spray at standard atmospheric conditions and Δp = 20 psi (138 kPa) while varying the diameter of the deflector and nozzle K-factor.

3.3 Stochastic Analysis

The stochastic model provides a more realistic view of the spray by predicting the initial drop size, locations and velocities. These distributions are important when dispersion and vaporization calculations are required such as in suppression modeling. Figures 10 - 12 show distributions for initial drop size, velocity and location for a sprinkler having $K = 3$ gal min^{-1} psi $^{-1/2}$, $D_{def} = 38$ mm. Turbulent intensities for the spray are also specified for the breakup process

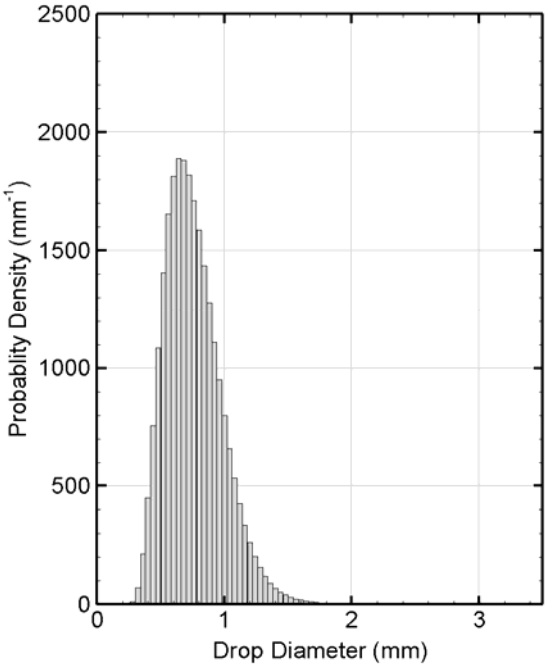

Figure 10. Probability density function of initial drop size determined from stochastic model, Δp = 20 psi, K = 3 gal min^{-1} psi $^{-1/2}$, D_{def} = 38 mm, $I_u = I_{sh} = I_{lig} = 0.2$.

describing the chaotic behavior of the velocity within the sheet ($I_u = 0.2$), the sheet fragmentation, ($I_{sh} = 0.2$), and the ligament fragmentation, ($I_{lig} = 0.2$). Figure 10 shows that the drop size distribution at these conditions is nearly Gaussian. The median drop size is 0.91 mm with minimum drop size of 0.24 mm and maximum drop size of 3.2 mm compared with a characteristic drop size of 0.77 mm predicted by the deterministic model. Figure 11 shows the initial velocity distribution ranges from about 4.4 to 25.0 m/s with a coarse Gaussian distribution. This choppy distribution results from the limited number of statistics available for velocity in this particular stochastic modeling approach. Initial locations for ligaments and drops are provided in Figure 12. It is apparent from

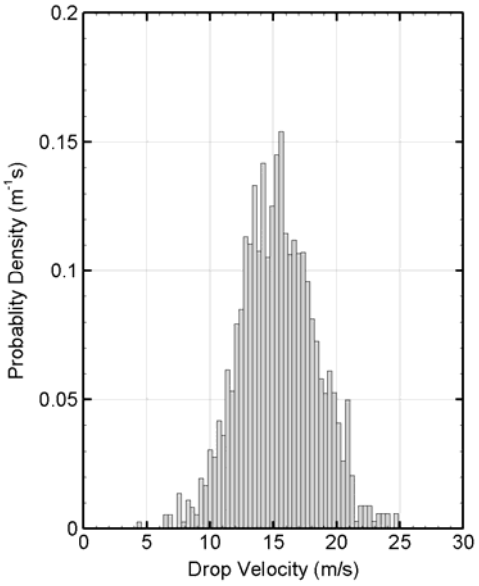

Figure 11. Probability density function of initial drop velocity determined from stochastic model, Δp = 20 psi, K = 3 gal min^{-1} psi $^{-1/2}$, D_{def} = 38 mm, $I_u = I_{sh} = I_{lig} = 0.2$.

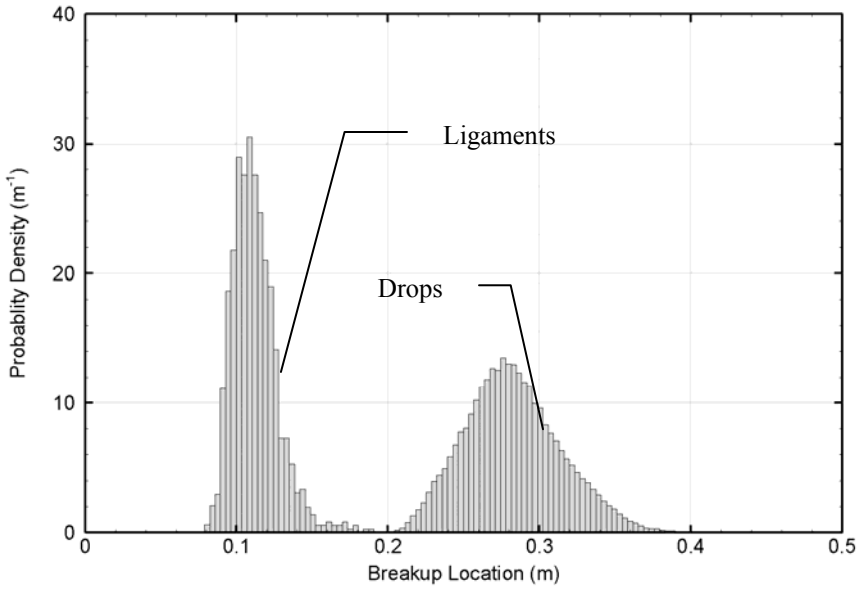

Figure 12. Probability density function of initial drop location determined from stochastic model, Δp = 20 psi, K = 3 gal min^{-1} psi $^{-1/2}$, D_{def} = 38 mm, $I_u = I_{sh} = I_{lig} = 0.2$.

this figure that drops do not initiate from one point, but result from a spatially distributed process. Figure 12 shows that the sheet breaks up into ligaments between approximately 0.08 m and 0.19m. In this region, the sheet or ligaments may be present. Ligaments begin to break up into drops at 0.20 m and continue to form drops until 0.49 m.

It is also useful to correlate the stochastic spray properties with drop size for specification of the initial spray in CFD modeling. In this approach, a range of characteristic drop sizes is defined representing the entire spray. The initial location,

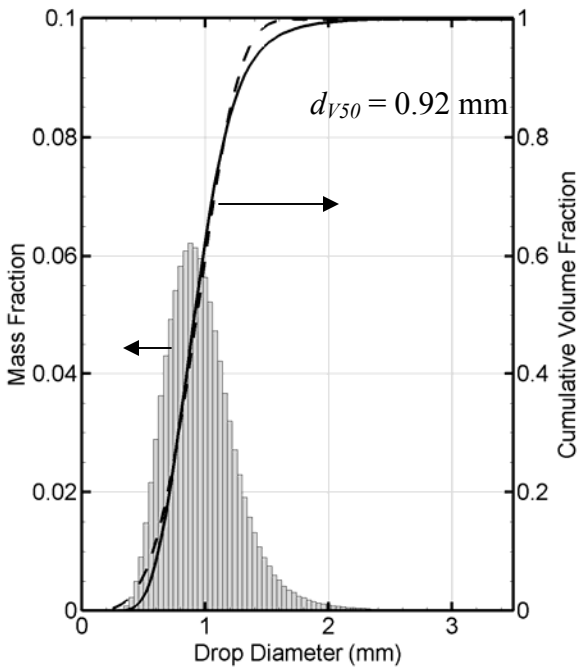

Figure 13. Mass/volume fraction for characteristic drop sizes predicted with the stochastic model, Δp = 20 psi, K = 3 gal min^{-1} psi $^{-1/2}$, D_{def} = 38 mm, $\overline{I_u} = I_{sh} = I_{lig} = 0.2$. Predicted cumulative volume fraction; Rosin-Rammler curve fit of prediction, X = 1.024, q = 3.90.

velocity, and mass fraction are then specified for each characteristic drop size in this distribution. This method allows for the entire spray to be specified and tracked using a relatively small number of drops. Figures 13 – 15 show the drop size based initial spray properties. Figures 14 and 15 show that the smallest drop sizes have the largest velocities and are formed at the earliest times. Figure 13 reminds us however, that these very small drops (as well as the very large drops) contain only a small fraction of the overall mass of the spray.

The drop size distribution is often provided in terms of the cumulative volume fraction. The cumulative volume fraction provides the percentage of the total spray

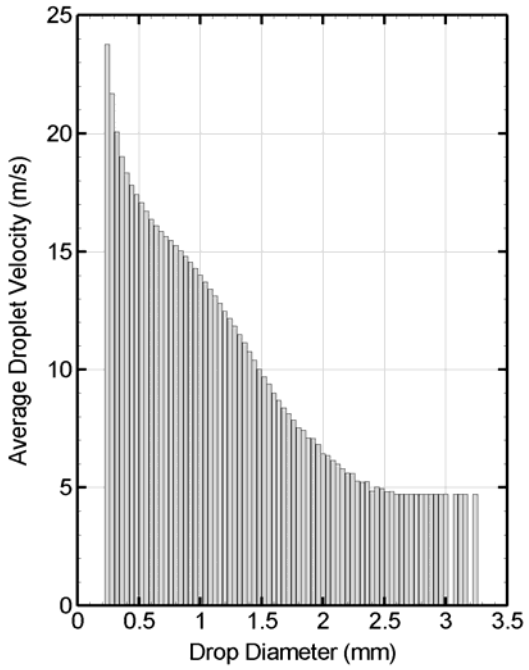

Figure 14. Velocities for characteristic drop sizes predicted with the stochastic model, Δp = 20 psi, K = 3 gal min^{-1} psi $^{-1/2}$, D_{def} = 38 mm, I_u = I_{sh} = I_{lig} = 0.2.

volume contained in drop sizes smaller than a specified drop diameter. The predicted cumulative volume fraction is provided in Figure 13. The Rosin-Rammler distribution has been found to represent the cumulative volume fraction for many real sprays. The Rosin-Rammler distribution is given by

$$CVF = 1 - e^{-(d_{CVF}/X)^q} \tag{3.1}$$

where CVF is the cumulative volume fraction of drops of diameter less than d_{CVF}, and X and q are empirical coefficients. The predicted cumulative volume fraction

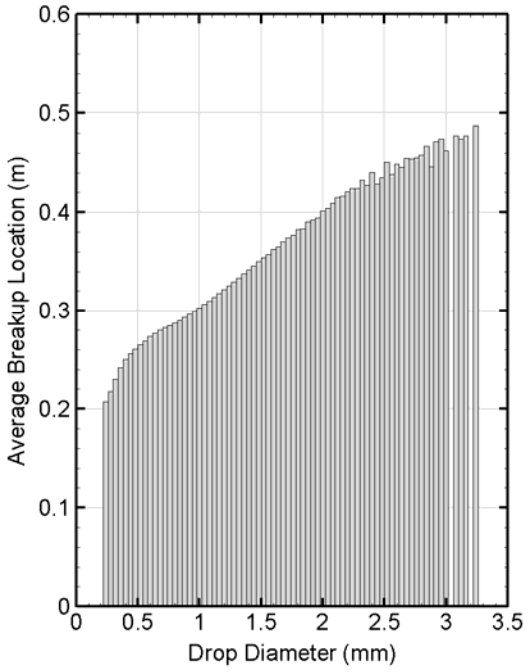

Figure 15. Initial drop locations for characteristic drop sizes predicted with the stochastic model, Δp = 20 psi, K = 3 gal min^{-1} psi $^{-1/2}$, D_{def} = 38 mm, $I_u = I_{sh} = I_{lig}$ = 0.2.

data is curve fit with the Rosin-Rammler expression to determine whether the predicted spray behaves like a typical spray and to determine the correlation coefficients X and q for the Rosin-Rammler distribution. The Rosin-Rammler

distribution having X= 1.024 mm and q = 3.9 compares well with the predicted spray, although the Rosin-Rammler distribution has slightly higher CVF for extreme drop sizes suggesting the predicted distribution may be somewhat narrow. This good agreement shows that the atomization model is capable of predicting drop size distributions, which are at least qualitatively consistent with those expected from real sprays.

In the Fire Dynamics Simulator, version 4 (FDS4), a combination of log-normal and Rosin-Rammler distribution, which is suggested by Factory Mutual based on their experimental results [3], is currently used to represent the Cumulative Volume Fraction (CVF) of the initial industrial sprinkler sprays,

$$CVF = \begin{cases} \dfrac{1}{\sqrt{2\pi}} \displaystyle\int_0^{d_{CVF}} \frac{1}{\sigma d} e^{-\frac{[\ln(d/d_{V50})]^2}{2\sigma^2}} dd & (d_{CVF} \le d_{V50}) \\ 1 - e^{-0.693\left(\frac{d_{CVF}}{d_{V50}}\right)^{\gamma}} & (d_{V50} < d_{CVF}) \end{cases} . \qquad (3.2)$$

The log-normal distribution is used to represent the CVF of the initial spray for the droplets that are smaller than the median volumetric diameter, d_{V50}, and the Rosin-Rammler distribution is used to represent the CVF for the droplets which are larger than the median volumetric diameter. The d_{V50}, σ and γ values are specified in the sprinkler file in FDS database based on the experimental data for a specific sprinkler. And in order to get a continuous CVF curve, σ *and* γ are related.

3.4 Spray Dispersion Analysis

By combining the atomization and particle tracking models, the distributed spray quantities and dispersion behavior could be calculated. In this study, the atomization model has been integrated into the FDS sprinkler model by replacing the spray specification sub-model used in FDS, and providing the initial droplet characteristics for the particle tracking sub-model in FDS. Important droplet properties such as the SMD, velocity, and mass flux of the spray have been output in Eulerian form at times and time ranges of interests. A post-processing program allows for time–averaging spray properties in Eulerian form.

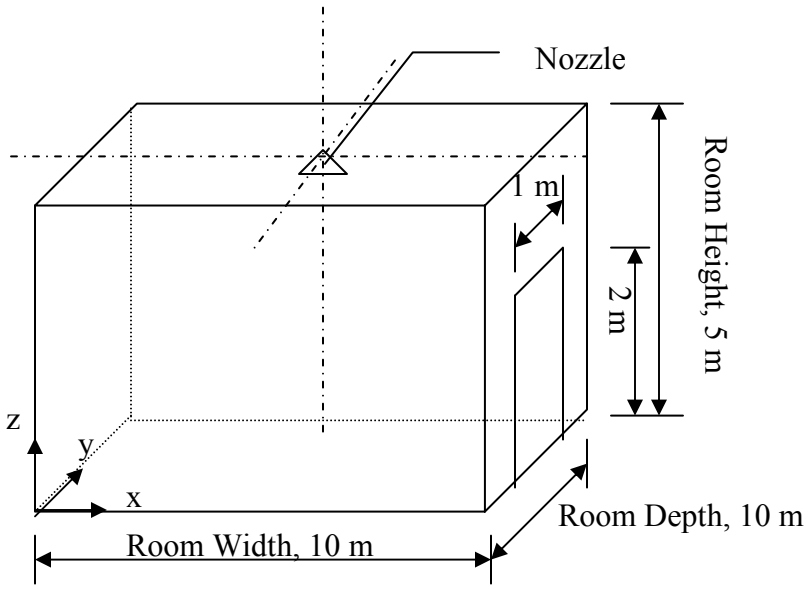

Figure 16. Schematic view of the test room simulated in FDS

The FDS is performed to simulate the spray dispersion in a concrete-walled enclosure (10m × 10m × 5m) with a 1m × 2m door open on the sidewall. The nozzle used in the simulations in this chapter is the ideal jet deflecting nozzle

described in the previous section having K = 3 gal min^{-1} psi $^{-1/2}$, D_{def} = 38 mm. The nozzle is placed 4.95m above the floor and it is in the center of the room. Figure 16 shows the computational domain of FDS and the position of the nozzle. In all the FDS tests, the nozzle is activated at the very beginning, and the keeps running for 180 seconds. The cell size used in the tests is 10 cm, suggested by J. Trelles [37], and 200 droplets are inserted into the computational domain every second. Actually, the higher droplets insertion rate, the better the spray would be represented. However, the computation expense increases significantly when increasing the number of droplets insertion rate.

3.4.1 Spray Dispersion in the Injection Plane

Based on the previous analysis, there is a strong coupling between the droplet atomization and the fire. The elevated temperature would change the initial spray characteristics. In order to visualize the effect of the elevated temperature on initial spray characteristics, two cases were tested by the modified FDS code, which use the atomization model to predict the initial spray characteristics. In the first case, the nozzle was running at room temperature, with an injection pressure equals to 20 psi; in the second case, the nozzle was running at an elevated temperature, 700K, with the same injection pressure. Simulations using elevated temperature could be used for predicting the distributed spray quantities under hot smoke layer condition. Figure 17a shows the predicted 120 seconds (60 s -180 s) averaged initial SMD distribution at the injection plane at room temperature, and

Figure 17b shows the predicted 120 seconds average SMD distribution at the injection plane at an elevated temperature.

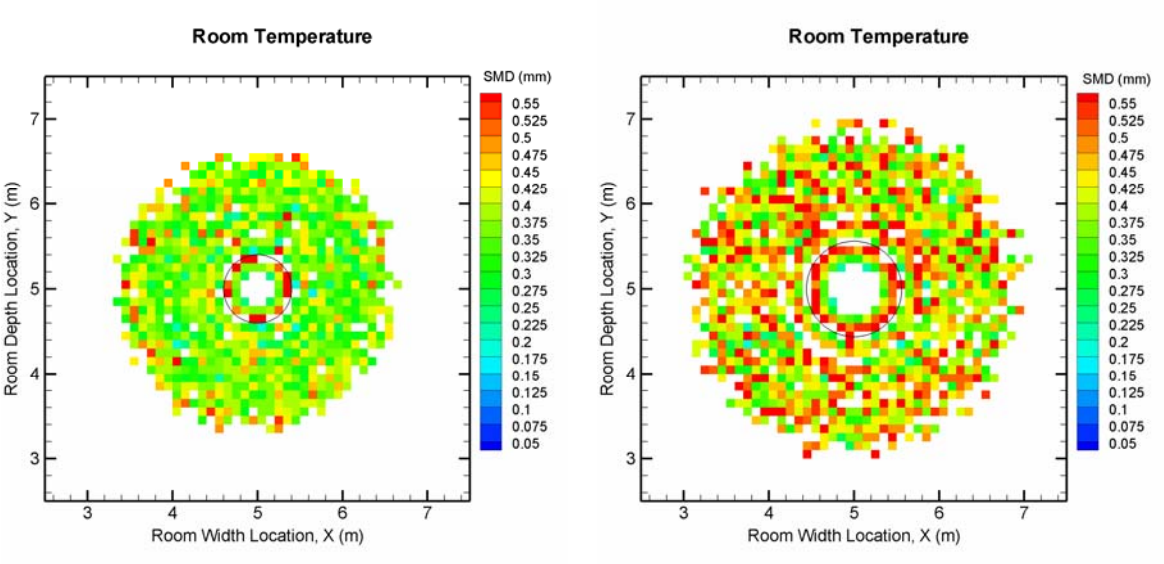

(a) (b)

Figure 17. (a) SMD distribution at the injection plane at room temperature, 293K. *(b)* SMD distribution at the injection plane at elevated temperature, 700K.

It could be seen that, in both cases, the smaller droplets tend to breakup closer to the center but the elevated temperature causes larger droplets breakup lengths and bigger droplet size. The changes in the initial spray characteristics would affect the spray dispersion behavior later.

Figures 18 a and 18b show the initial velocity distribution at the injection plane at room temperature and elevated temperature respectively. It can be seen that the overall predicted droplet velocities in the elevated temperature are larger than the predicted droplet velocities in the room temperature. And it should be noted that in both cases, in the atomization region which is about less than 0.5m from the center of the nozzle, the droplet velocity could be up to 20 m/s, but

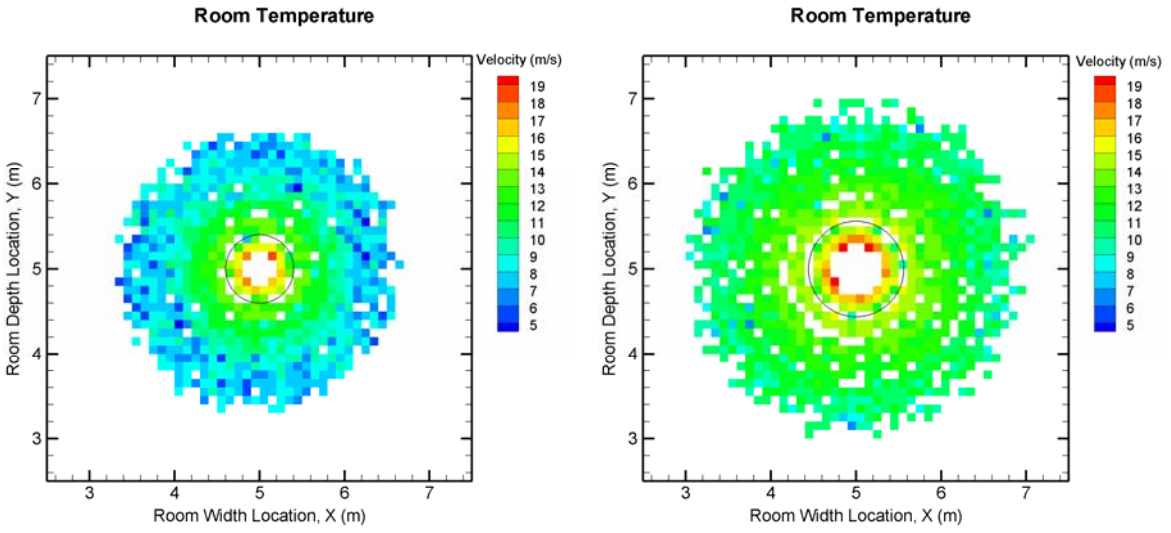

(a) (b)

Figure 18. (a) Velocity distribution at the injection plane at room temperature, 293K. *(b)* Velocity distribution at the injection plane at elevated temperature, 700K.

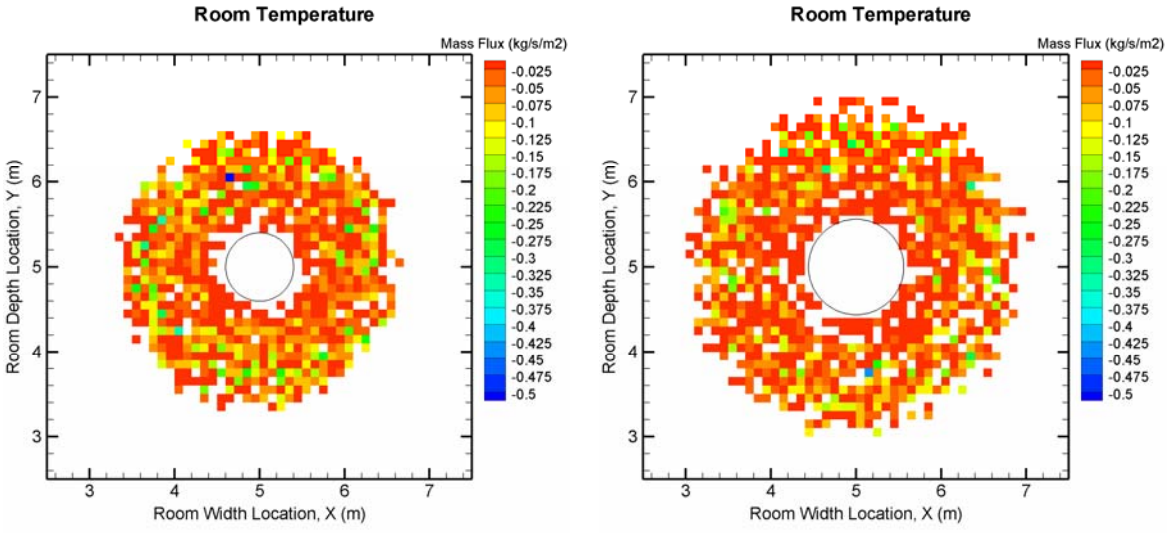

(a) (b)

Figure 19. (a) Water mass flux distribution at the injection plane at room temperature, 293K. *(b)* Water mass flux distribution at the injection plane at elevated temperature, 700K.

beyond the atomization model, the droplet velocity would drop down to 10 m/s. Moreover, if Figures 17 a and b and Figures 18 a and b are looked at together, it could be seen that smaller droplets have larger initial velocities, which is consistent with the previous analysis in the atomization model. These results show that the droplets decelerate significantly after formation, because of the drag force from the air, especially for the smaller droplets.

Figures 19 a and 19b show water mass flux distribution at the injection plane at room temperature and elevated temperature respectively, water mass flux is a very important parameter to study fire suppression, it represents where the water goes. Total mass flux in each plane at different elevations is examined to evaluate the quality of spatial and time averaging. At room temperature, when the droplet vaporization is not significant, the total mass flux at each plane is conserved with the jet flow rate. Elevated temperature results in more drop vaporization.

3.4.2 Spray Dispersion on the Floor

The distributed spray quantities in horizontal planes change with elevation. Figure 20-22 shows the predicted 120 seconds (60s -180s) averaged SMD, velocity and mass flux distributions of the spray generated by the ideal jet deflecting nozzle, having K = 3 gal min^{-1} psi $^{-1/2}$, D_{def} = 38 mm, on the plane near the floor at room temperature with the injection pressure equals to 20 psi. By looking at the distributed spray quantities on the floor plane, it could be seen that the droplets that have larger droplet sizes have larger velocities and move farther away from the centerline of the nozzle, and contribute more mass flux. However, the droplet

velocities decrease significantly compared with the initial droplet velocities during the dispersion process. It could be extrapolated that if there were a fire in the room with a fire plume going upward, the velocity of the droplets would decrease even faster. Another thing should be noted is that the 120 seconds averaged predicted spray on the floor is very sparse, which means there is some place on the floor that no droplets would hit on during 120 seconds. This unrealistic result is due to the limited number of droplets used to represent the entire spray. The predicted results could be better by using more representative droplets at the expense of computational time. As a result, the number of droplets that used to represent the spray should be chosen wisely, considering both prediction accuracy and computation expense.

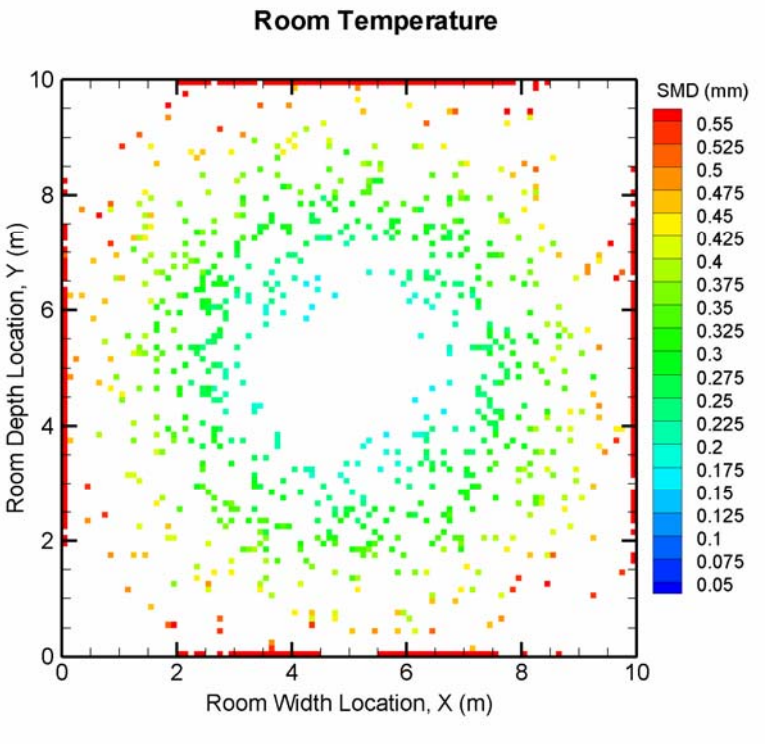

Figure 20. SMD distribution on the floor plane at room temperature, 293K.

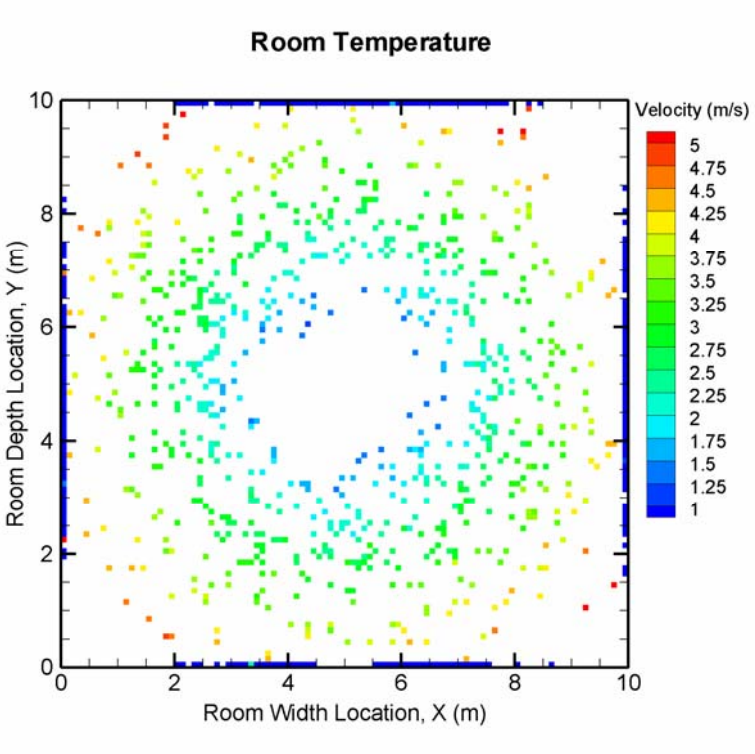

Figure 21.Velocity distribution on the floor plane at room temperature, 293K.

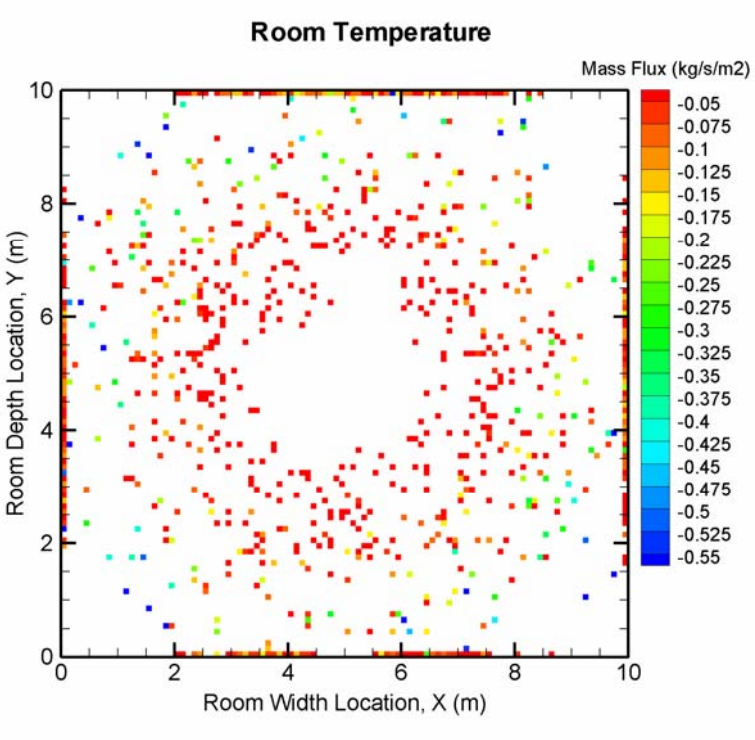

Figure 22. Mass flux distribution on the floor plane at room temperature, 293K.

3.4.3 Spray Dispersion on Vertical Plane

The dispersed droplet distributions of the spray in a vertical plane could clearly show the spray dispersion behavior for the entire spray. Figures 23-25 show the predicted 120 seconds averaged SMD, velocity and mass flux distributions at the vertical x-z plane across the center of the nozzle (y = 5.0 m) for the same spray described in the previous section at room temperature. It could be clearly seen that the shape of the predicted spray is very hollow and smaller droplets are closer to the centerline of the nozzle. The hollow shape of the spray is partially because of that the spray is generated by the ideal jet deflecting nozzle. For the real sprinkler or low to medium water mist nozzle, there are likely to be tines on the deflector, the spray would be less hollow. It could also be seen that the smaller droplets have larger initial velocities, but they decelerate much faster than the bigger ones, they stay closer to the

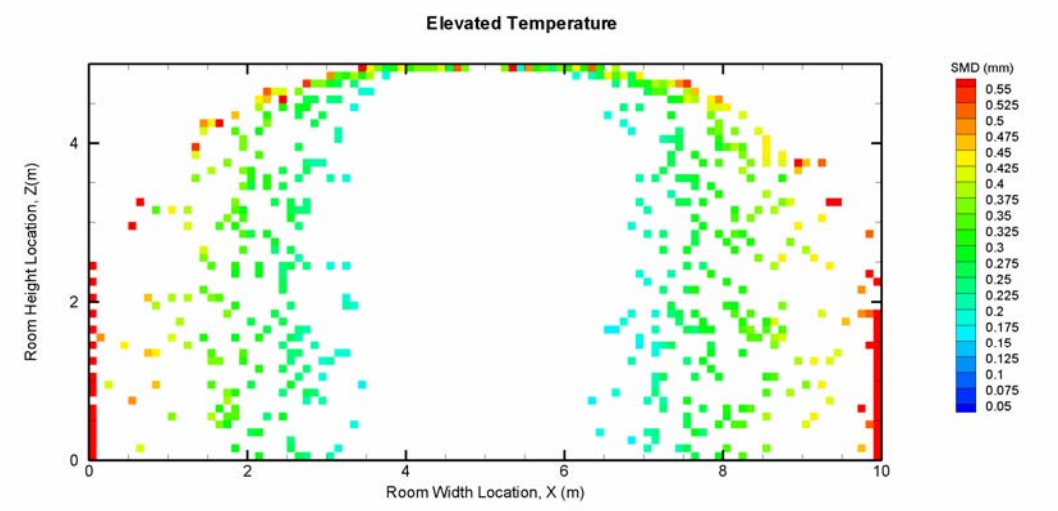

Figure 23. SMD distribution on the vertical plane in the center of the room at room temperature, 293K.

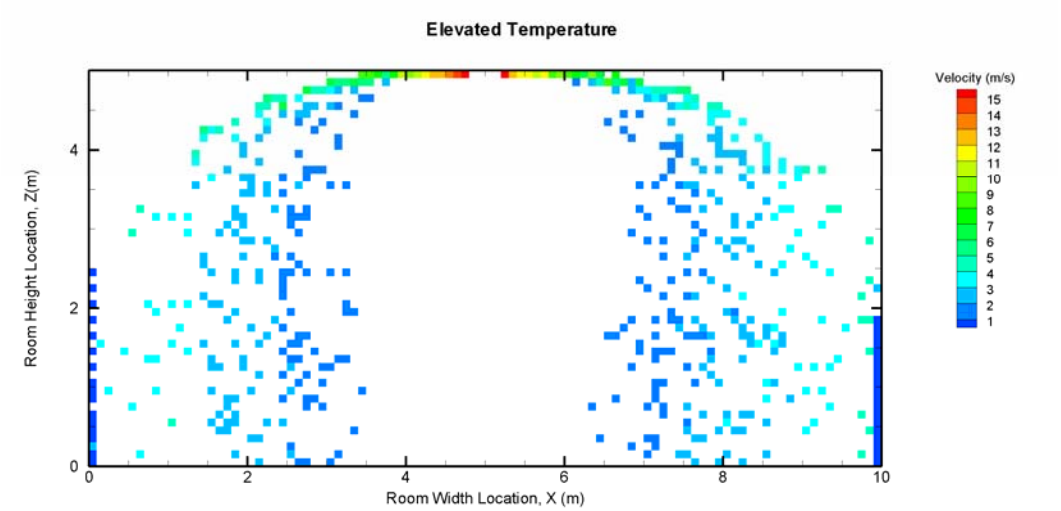

Figure 24. Velocity distribution on the vertical plane in the center of the room at room temperature, 293K.

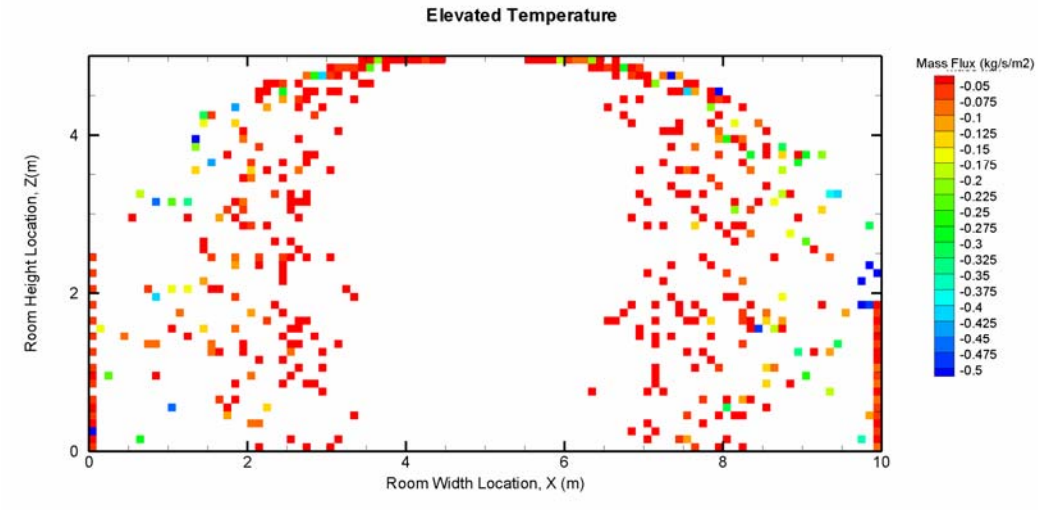

Figure 25. Mss flux distribution on the vertical plane in the center of the room at room temperature, 293K.

centerline of the spray. Clearly the smaller droplets have smaller momentum, so they are less likely to be able to penetrate into the fire plume but they would be easily entrained into the plume with the air.

3.4.4 Effect of Initial Spray Specification on Spray Dispersion at Elevated Temperature

As discussed in chapter 1 and 2, normally the CFD models use empirical distributions as well as some other simple correlations which have been developed for estimating characteristic drop sizes based on a few experiments. However, the data in these correlations are obtained under quiescent 'cool' conditions, but the elevated temperatures in real fires are expected to influence the atomization process. The atomization model developed in this study accounts for the effect of the elevated temperature on the atomization process, which has been shown in the previous sections. In order to see how important it is to account for the effect of elevated temperature on the atomization process, the spray dispersion behavior should be evaluated. Two cases were tested using modified FDS code, and the test configurations are the same which has been described at the beginning of section 3.4, and the two cases were tested at elevated temperature of 700K. Droplet vaporization is considered in both of the two cases. The difference in these cases is the initial spray specification: in the first case, the initial spray is specified using the predicted results by the atomization model at 700K, while in the second case, the initial spray is specified using the predicted results by the atomization model at room temperature 293K. In the first case, the effect of the elevated temperature on the atomization process is accounted for, but the effect is not accounted for in the second case. As a result, the predictions obtained in the first case would be more realistic than in the second one. Figures 26 a and b show

the predicted 120 seconds averaged SMD distribution at the vertical x-z plane across the center of the nozzle (y = 5.0 m) for the spray generated in the two cases.

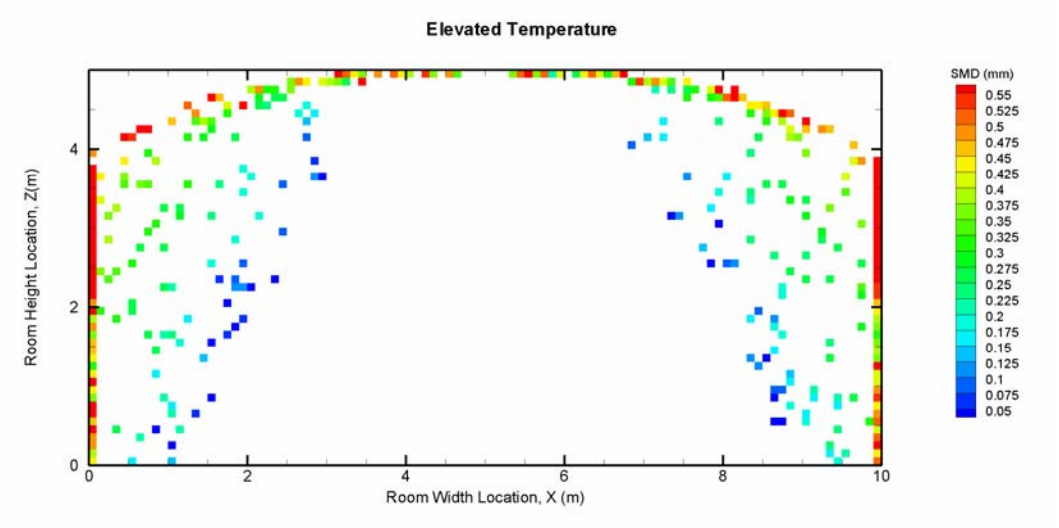

(a)

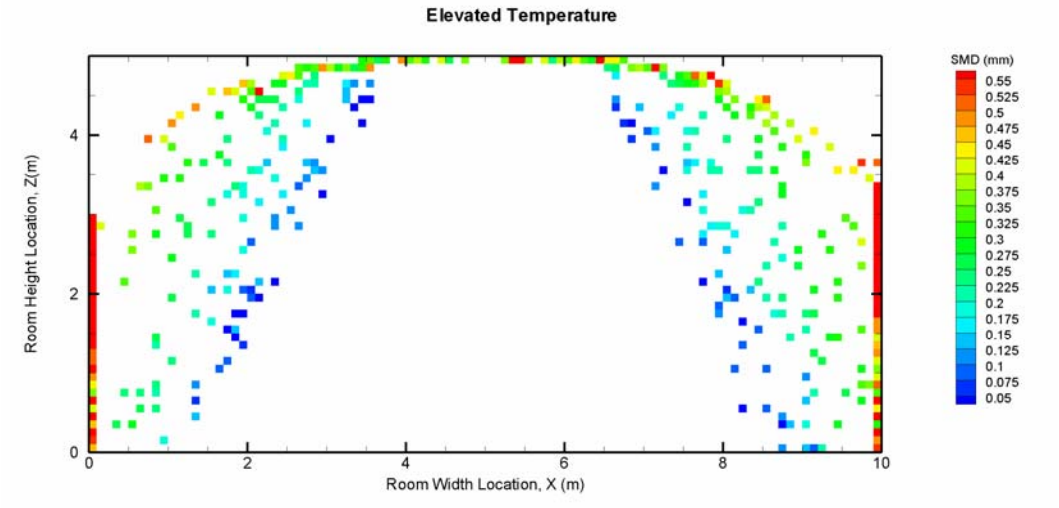

(b)

Figure 26. (a) SMD distribution on the vertical plane in the center of the room at elevated temperature, 700K, with initial spray characteristics predicted at elevated temperature. *(b)* SMD distribution on the vertical plane in the center of the room at elevated temperature, 700K, with initial spray characteristics predicted at room temperature.

Figures 26a and b show that if we include the effect of the elevated temperature on the initial spray, the shape of the spray becomes hollower, more droplets hit the wall at a higher elevation, and the overall droplet sizes increase. As a result, where the water would go changes. Figures 27 a and b show the mass flux distribution at the plane 2.5m above the floor for the two cases with different initial spray specifications.

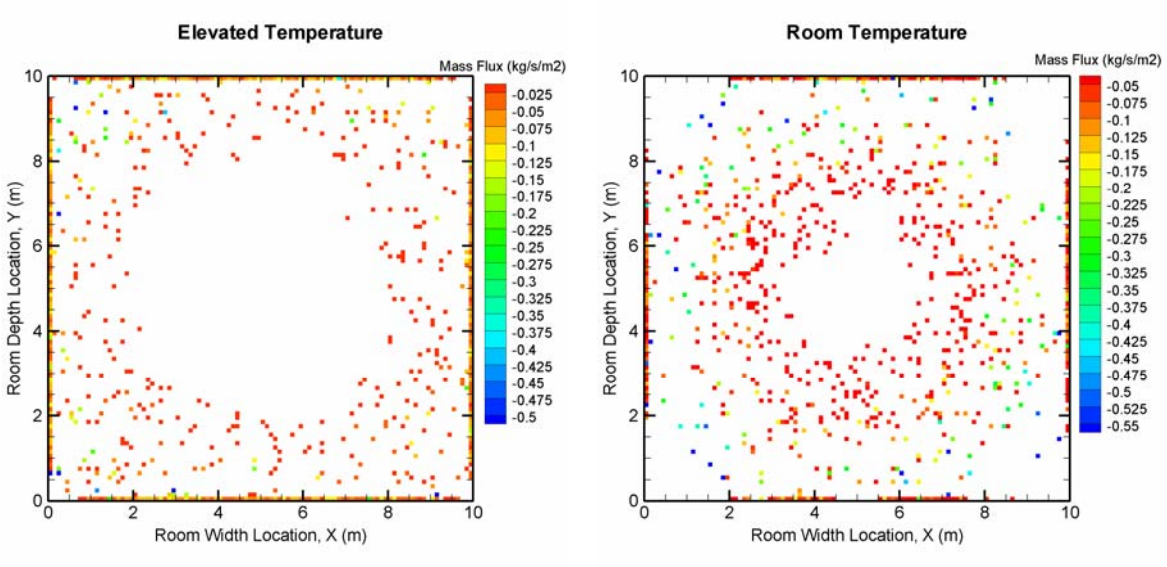

(a) (b)

Figure 27. (a) Water mass flux distribution at the plane 2.5m above the floor at elevated temperature, 700K, with initial spray characteristics predicted at elevated temperature. *(b)* Water mass flux distribution at the plane 2.5m above the floor at elevated temperature, 700K, with initial spray characteristics predicted at room temperature.

Figures 27a and b clearly show the effect of initial spray specification on the spray dispersion behavior. As a result, if the CFD spray models, which specify the initial spray by the experimental data measured in a cool and quiescent condition, are used to predict the performance of a water based fire suppression device, the

effectiveness of the suppression device would not be well predicted, because actually the amount water that get into the fire changes because of the strong effect of the elevated temperature on the atomization process.

In the spray dispersion analysis, the distributed spray properties such SMD, droplet velocities and the water mass flux have been visualized at different elevations. It could be seen that the smaller droplets tend to have a larger initial velocity, however, they decelerate much faster than the bigger droplets, so they would be closer to the centerline of the nozzle later on. The spray generated by the ideal jet deflecting nozzle is pretty hollow, that means in a real fire, it may not be the most effective if the nozzle is right above the fire. It could be also clearly seen by integrating the atomization model into FDS, the modified FDS program is able to account for the strong coupling between the fire and the spray.

In this study, fire was not introduced in the spray dispersion analysis, so whether the modified FDS program which includes the atomization model could provide a better prediction of the water-based fire suppression system performance is unknown. However, the effect of elevated temperature on the spray properties was considered, and it is possible to compare the predictions by the model with experimental data obtained in a quiescent condition. It stands to reason that if the model could provide a better prediction of spray properties in a quiescent condition, it will also get a better prediction for the water-based fire suppression system performance in a real fire.

3.5 Model Validation

In the previous analysis, the CVF predicted by the atomization model shows a good agreement with the Rosin-Rammler distribution, which is usually used to represent a real spray. That means the model is capable of predicting drop size distributions, that are at least qualitatively consistent with those expected from real sprays. A more quantitative evaluation of the model performance was obtained by comparing model predictions with actual sprinkler measurement data or with the empirical correlations obtained from actual sprinkler data. Since the initial drop distribution will be distributed in space as the spray dispersed, the initial drop size distribution should be compared with overall drop size distribution measured in a plane, assuming that the vaporization at room temperature is negligible and negligible secondary atomization.

3.5.1 Comparison with Early Measurements

A quantitative evaluation of the model performance was obtained by comparing model predictions with the empirical correlations obtained from actual sprinkler data. The relative invariance in drop size measurements at different elevations in You's study [3] suggests that secondary atomization is not important, allowing initial predictions of drop size to be compared with downstream measurements. Figure 28 shows the modeling predictions compared with data provided by Dundas [4]. Dundas showed that data from many sprinklers could be correlated by

$$\frac{d_{V50}}{D_{orif}} = C\ We^{-1/3}, \tag{3.3}$$

where 50% of the spray volume is contained in drops smaller than d_{V50} (volume median diameter). In Dundas' research, the correlation coefficient for pendant sprinklers having D_{orif} = 12.7 mm and D_{def} = 31 mm was determined to be C = 3.1. Model drop size predictions for pendant sprinklers with similar geometry were compared to the experimental data and corresponding correlation at various injection pressures. These model predictions agree very well with the experimental data and correlation curve. The model prediction used turbulence intensities of I_u = 0.2, I_{sh} = 0.2, I_{lig} = 0.2 for all We. These turbulence intensities

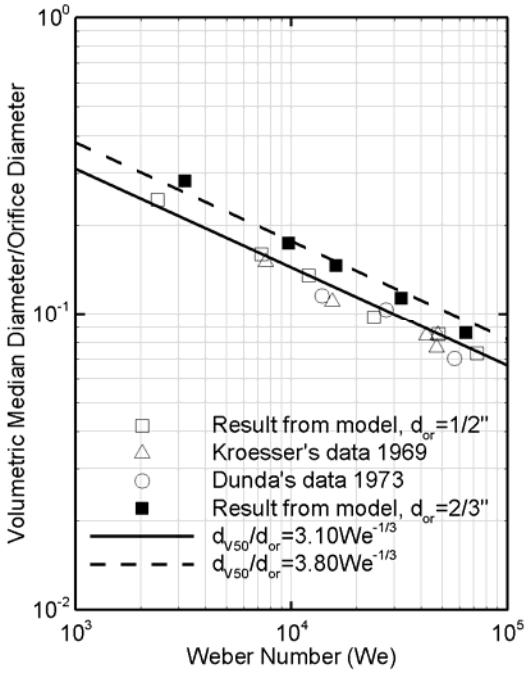

Figure 28. Comparison between the stochastic model predictions with correlation obtained from sprinkler data.

were set somewhat arbitrarily; however, they appear to have reasonable values. Better guidance for these values will be obtained as more detailed data in the breakup region of the spray is obtained. The authors are currently conducting spray measurements in this region to build models for determining these turbulence intensities. You also suggested that the correlation coefficient C depends on the diameter of the nozzle orifice from his experimental data, the larger the nozzle orifice diameter is, the bigger the coefficient C is. As a result, the d_{V50} of the spray generated by a nozzle with a larger orifice diameter at different injection pressures are predicted by the stochastic atomization model, which is shown in figure 28. The correlation coefficient for this pendant sprinklers having D_{orif} = 16.9 mm and D_{def} = 31 mm was determined to be C = 3.8. The trend of the coefficient predicted by the stochastic model is the same as the trend obtained in You's experiments.

3.5.2 Comparison with Advanced Sprinkler Measurements

In the previous section, the stochastic model predictions of d_{V50} for real sprinkler spray generated by different injection pressures show a good agreement with early measurements and the empirical correlations. It would be more quantitative to compare the predicted droplet size distribution with droplet size distribution measurements. Sheppard used PDI technology to characterize the droplet size distribution for a set of commercial available sprinklers. He measured the drop size distribution close to the sprinkler (0.38m away from the sprinkler), at a single azimuthal angle which is almost perpendicular to the frame arm, but at

different elevation angles. Recall that the initial drop distribution will be distributed in space as the spray dispersed, the initial drop size distribution should be compared with the overall drop size distribution measured in the spray. Sheppard provided the droplet size measurements for a sprinkler, P13B, having K = 5.6 gal min^{-1} psi $^{-1/2}$, D_{def} = 27 mm, at Δp = 88KPa (12.8 psi). He measured the droplet size distribution at four elevation angles, $\theta = 0^o$, 10^o, 30^o, and 60^o. Sheppard also measured the average velocities of the spray at these four elevations, which could be used to estimate the mass flux at different elevation angles. So in order to get the overall droplet size distribution for the spray, the

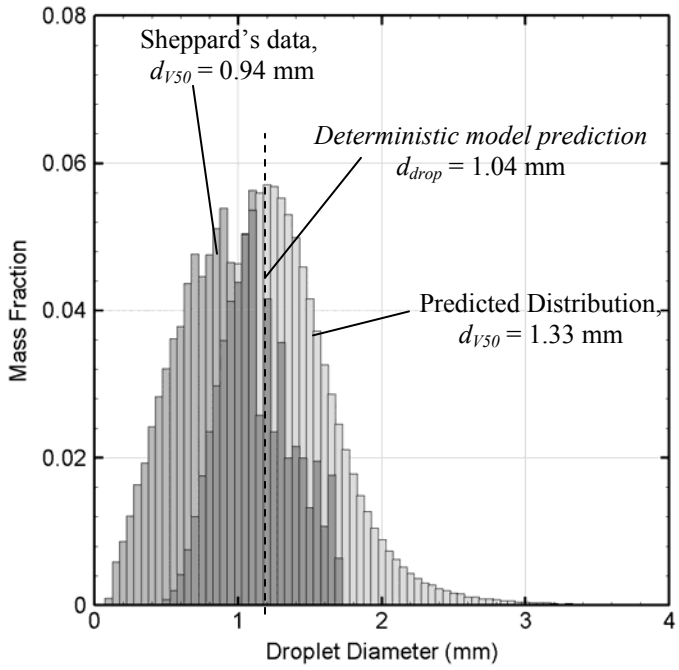

Figure 29. Comparison between the droplet mass fraction distribution predicted by the stochastic model with Sheppard's measurements.

droplet size distributions at different elevation angles are averaged by velocity, which is actually averaged by mass. The overall droplet mass fraction distribution measured by Sheppard is shown in Figure 29. And the predicted droplet size mass fraction distribution by the stochastic model for the same sprinkler is obtained by using turbulence intensities of $I_u = 0.2$, $I_{sh} = 0.2$, $I_{lig} = 0.2$. The predicted d_{V50} is larger than the d_{V50} measured in the experiment, and it seems that the model doesn't predict as many small droplets as measured in the experiments. There are two possible reasons that may cause the discrepancy. First, the atomization model is based on the wave dispersion theory, only the wave instability breakup mechanism has been considered, however, there are other droplet breakup mechanisms such as stripping breakup and bag breakup, so it may cause the model to fail predicting small droplets. Even for the wave instability breakup mechanism, the empirical criterion for predicting sheet breakup, $f_{crit,sh}$ =12, may not be necessarily accurate. Second, the model is developed based on a simple geometry, but there are tines on the real sprinkler, so smaller droplets would be generated by the real sprinkler. These two model limitations have already been addressed in Chapter 2. However, there may also be error in measured droplet size distribution in Sheppard's experiment. The predicted d_{V50} by the stochastic model agrees with Dundas' empirical correlation very well, but the coefficient for the correlation obtained using Sheppard's data is much lower than 3.1, which is obtained by Dundas. That may be because Sheppard only measured the droplet size distribution at one azimuthal, but it is highly likely that the droplet size distribution changes significantly with azimuthal angle. As a result, the overall

droplets size distribution for the entire spray would be more accurate if obtained by averageing among measurements at different azimuthals.

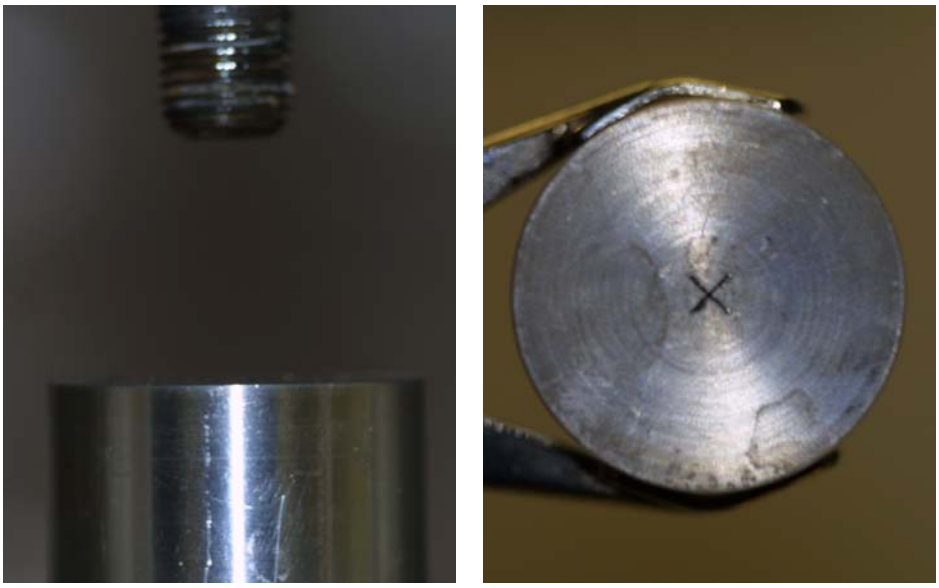

Figure 30. Photo of ideal jet deflecting injector, K = 3 gal min-1 psi -1/2 , Ddef = 38 mm.

Spray characterization experiments for ideal jet deflecting injector, which has been used in the model before, were also conducted in University of Maryland, Fire Protection Engineering department using Malvern Drop Size Analyzer. Figure 30 shows the picture of the ideal injector: The droplet size distributions of the spray generated by this ideal injector at different injection pressure, which is ranging from 5 psi to 30 psi, were measured by the Malvern Droplet Size Analyzer. A schematic of this instrument is shown in Figure 31. It is a spatial sampling device based on laser

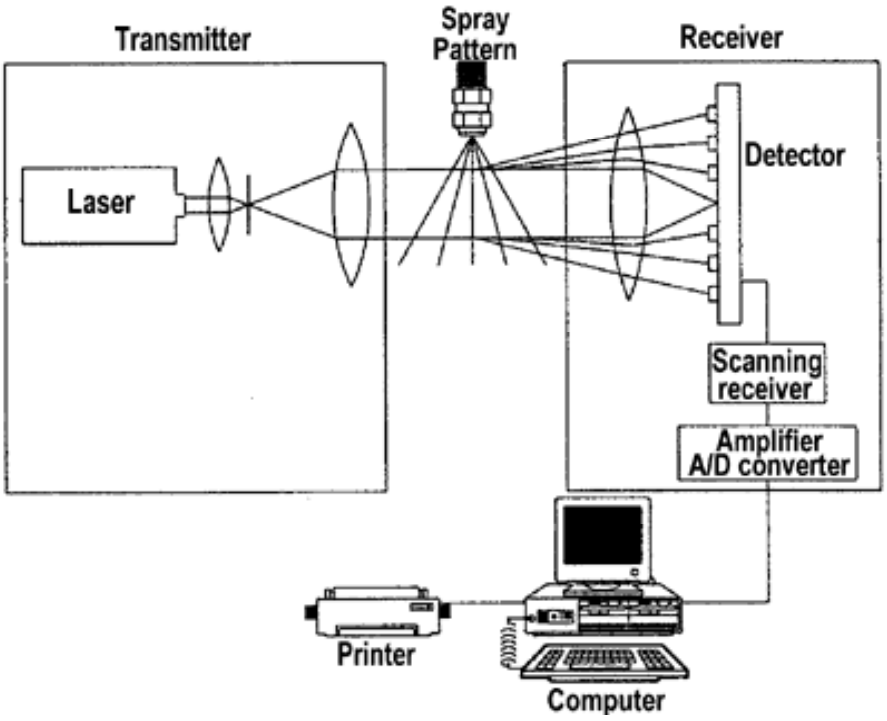

Figure 31. Schematic of the Malvern drop size analyzer.

diffraction. The laser passing through the spray is scattered. The scattered light intensity is measured using annular photodiodes. Then a curve fitting program is used to convert the light intensity distribution into any of several empirical drop size distribution functions. One of the limitations is the multiple scattering that may occur when the spray density is too high. However programs are used to correct the drop size distribution.

In order to compare the experimental results with the predictions from the atomization model, the measurements were taken at the injection plane, which is at the same elevation as the deflector of the injector, and 0.65m away from the centerline of the injector. The d_{V50} measured by the Malvern at different injection pressures are much lower than the predicted values by the stochastic model using

turbulence intensities of $I_u = 0.2$, $I_{sh} = 0.2$, $I_{lig} = 0.2$, and the measured d_{V50} is proportional to $p^{-1/3}$, which is proposed by Dundas[4]. There are several possible causes for the discrepancy, first, because the model doesn't include other sheet and ligament breakup mechanism, it may be due to the lack of the capability for predicting the small droplets; second, the measurement for droplet size distribution at each injection pressure has only been conducted at one particular position, assuming the spray is symmetric, so the measured drop size distribution is obtained by averaging among a small volume of spray, it may not well represent the entire spray. Another important reason to account for the discrepancy is the sampling technique used by Malvern. There are two different types of drop size sampling techniques [38]. One is known as spatial averaging and the other is called flux averaging. With the spatial techniques, a collection of droplets occupying a given volume is sampled instantaneously. This type of measurement is sensitive to the density in each class size and to the number of particles per unit of volume. The flux technique is implied when individual droplets that pass through the cross section of a sampling region are examined during an interval of time. Generally flux measurements are collected by optical measurements that are capable of sensing individual drops. The flux technique does not provide the same values as spatial technique. Indeed flux values are biased by the velocity profile of the spray. For instance if small drops have a higher velocity than big drops the flux technique will see through its cross-section a lot more small droplets than spatial technique. So the mean diameter of the

droplets provided by the flux technique will be bigger than spatial technique. Malvern and the modified distribution using velocity profile at Δp = 20 psi..

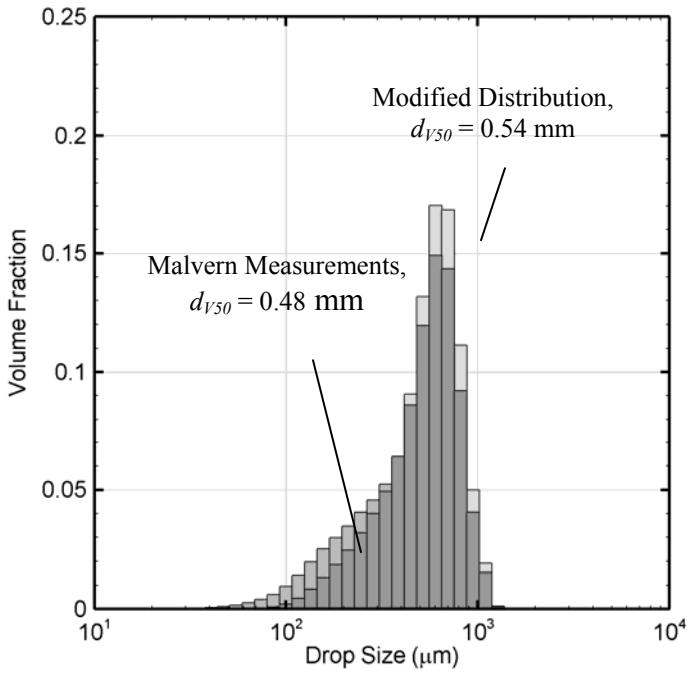

Figure 32. Comparison between measured drop size distribution with modified experimental results, Δp = 20 psi.

Since the predicted initial droplet size distribution is biased by the velocity profile of the spray, however, the Malvern measurements use the spatial technique, the droplet size distribution measured by the Malvern should be weighted by velocity profile in order to compare with the predicted distribution by stochastic model. The initial droplet velocity, V = 15.24 m/s, initial droplet location r = 0.288 m calculated by the deterministic model at Δp = 20 psi is assumed to be initial velocity and initial location for the measured droplet. Then the velocity of the droplet at r = 0.65, is estimated by the following equations[5]:

$$\frac{\partial V_d}{\partial t} = -\frac{3\rho_g}{4d\rho_l} C_d V_d^{\,2} \tag{3.3}$$

where

$$C_d = \frac{24}{\mathrm{Re}} \qquad \mathrm{Re} < 1 \tag{3.4}$$

$$C_d = \frac{24}{\mathrm{Re}} + \frac{6}{1+\sqrt{\mathrm{Re}}} + 0.4 \qquad 1 < \mathrm{Re} < 10^5 \tag{3.5}$$

The small droplets decelerate extremely quickly, so that at r = 0.65 m, the larger droplets travel much faster than the small droplets. After modifying the droplet size distribution by the velocity profile, the d_{V50} goes up from 0.48mm to 0.54 mm. Figure 32 shows the droplet mass fraction distribution measured by the Malvern and the modified distribution using velocity profile at Δp = 20 psi.

Furthermore, Figure 33 shows the comparison between the droplet mass fraction distribution predicted by the stochastic model with the modified experimental results when Δp = 20 psi. The predicted droplet sizes are still much bigger than the measured droplet size after modifying the distribution with velocity profile, however, these two figures reveal that the sampling technique plays an important role in the drop size characterization The initial droplet size distribution predicted by the atomization model should be compared with measurements using flux sampling technique, but the droplet size distribution calculated by the modified FDS could be compared with Malvern measurements directly. Unfortunately, the distributed spray properties could not be obtained using the current spray chamber experiment facility, more full scale spray testing data are needed to validate the atomization model and the dispersion model

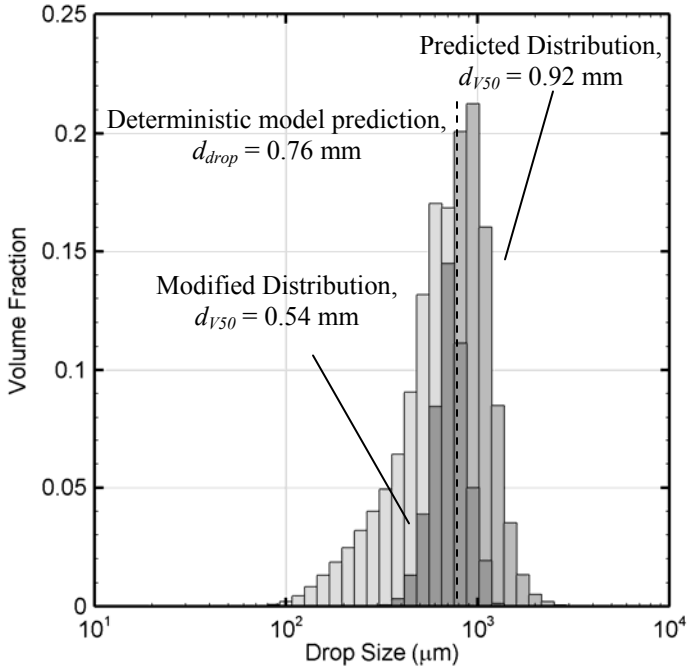

Figure 33. Comparison between predicted drop mass fraction distribution by the stochastic model using $I_u = I_{sh} = I_{lig}$=0.2 with modified experimental results, Δp = 20 psi.

Chapter 4: Conclusions

An atomization model for water based suppression devices, including conventional sprinklers and low-medium water mist nozzles, has been developed based on free surface boundary layer and wave dispersion theories. The nozzle is modeled as an impinging jet. The effect of the frame arms and tines are not currently incorporated into the model, but will be included in future refinements. The sensitivity of the atomization process to operating conditions, such as the injection pressure, ambient gas temperature, and nozzle geometries has been addressed using a deterministic model, and the distributed initial spray properties, which include the initial drop size distribution, drop velocity distribution and the drop location distribution, could be predicted by the stochastic model. The atomization model predicts an initial spray having a realistic drop size distribution, which closely matches the Rosin-Rammler expression. Median volume diameters, d_{V50}, and the shape of the droplet distribution calculated from predicted distributions show good agreement with actual drop size measurements from sprinklers.

Since the atomization model provides initial velocities, locations, and mass fractions that can be used to track an array of characteristic initial drop sizes that represent the entire spray, it has been integrated with the dispersion model using in FDS 4.0. The spray properties at the atomization region and the spray dispersion behavior have been visualized using the post process program developed in this study. The predicted result shows that small droplets have a larger velocity in the atomization region, but they decelerate much faster than the

larger ones do. Larger droplets move farther away from the centerline of the nozzle, which results in a bigger water mass flux. The effect of the initial spray specification on the spray dispersion behavior has also been addressed, and the importance of including the strong coupling between the elevated temperature and the spray in the spray atomization process has been established.

Bibliography

[1] Grant, G., Brenton, J., and Drysdale, D., "Fire Suppression by Water Sprays," *Progress in Energy and Combustion Science*, Vol. 26, pp. 79-130, 2000.

[2] Marshall, A. W. and Guillemin, D., "An Analytical Model for Prediction Initial Spray Properties from Liquid Suppression Devices," *Workshop on Fire Suppression Technologies Proceedings*, Mobile, AL, 2003.

[3] You, H. Z., "Investigation of Spray Patterns of Selected Sprinklers with the FMRC Drop Size Measuring System," *First International Symposium on Fire Safety Science,* New York, pp. 1165-1176, 1986.

[4] Dundas, P. H., "Technical Report Optimization of Sprinkler Fire Protection The Scaling of Sprinkler Discharge: Prediction of Drop Size," FMRC Serial No. 18792 RC73-T-40, *Factory Mutual Research Corporation*, Norwood, MA, June 1974.

[5] Sheppard, D. T., "Spray Characteristic of Fire Sprinklers," NIST GCR 02-838, *National Institute of Standards and Technology*, Gaithersburg, MD, 2002.

[6] Lawson J. R., Walton W. D., and Evans, D. D., " Measurement of Droplet Size in Sprinkler Sprays", National Bureau of Standards, U.S. Department of Commerce, NBSIR 88-3715, Gaithersburg, MD, Feb. 1988.

[7] Nolan P. F., "Feasibility Study of Using Laser High Speed Cine System for the Characterization of Droplets from Sprinkler Sprays", The Swedish Fire Research Board, Stockholm, Sweden, 1989

[8] Jackman. L. A., Nolan P. F., Morgan H. P. "Characterization of Water Drops from Sprinkler Sprays", Fire Suppression Research – First International Conference, Stockholm, Sweden, 1992.

[9] Chow W. K. Shek L. C., "Physical Properties of a Sprinkler Water Spray", Fire Mater, Vol. 17, pp. 279-292, 1993.

[10] Chan T. S., "Measurements of Water Density and Drop Size Distributions of Selected ESFR Sprinklers", Journal of Fire Prot Engr, Vol. 6, pp. 79-87, 1994.

[11] Putorti A. D. Belsinger T. D., and Twilley W. H. " Determination of Water Spray Drop Size and Speed from a Standard orifice, Pendent Spray Sprinkler", Report of Test. NIST, Gaithersburg, MD, May 1999.

[12] Heskestad, G., "Proposal for Studying Interaction of Water Sprays with Plume in Sprinkler Optimization Program," Memorandum to C. Yao, June 16, 1972.

[13] Widmann, J. F., "Phase Droppler Interferometry Measurements in Water Sprays Produced by Residential Fire Sprinklers", *Fire Safety Journal*, Vol. 36, pp. 545-567, 2001.

[14] Widmann, J. F., Sheppard, D. T., and Lueptow, R. M., "Non-Intrusive Measurements in Fire Sprinkler Sprays", *Fire Technology*, Vol. 37, pp. 297-315, 2001.

[15] Bachalo W. D., "Experimental Methods in Multiphase Flows", *International Journal of Multiphaee Flow*, Vol. 20, pp. 261-295, 1994

[16] Adrian, R. J., "Doule Exposure, Multiple-Field Particle Image Velocimetry for Turbulent Probability Density", *Optics and Lasers in Engineering*, Vol. 9, pp. 211-228, 1988

[17] Adrian, R. J., "Particle – Imaging Technoques for Experimental Fluid Mechanics", *Annu. Rev. Fluid Mech*., Vol. 23, pp. 261-304, 1991

[18] Westerweel, J., "Fundamentals of Digital Particle Image Velocimetry", *Meas. Sci. Technol.* Vol. 8, pp. 1379-1392, 1997

[19] Reitz, R. D., and Bracco, F. V. "Mechanism of Atomization of a Liquid Jet", *Physics of Fluids*, Vol. 25, pp. 1730-1742, 1982.

[20] Chang, I. D., and Russell, P. E., "Stability of a Liquid Layer Adjacent to a High-Speed Gas Stream", *The physics of Fluids*, Vol. 8, pp. 1018-1026, 1965.

[21] Lian, Z. W., and lin, S. P., "Breakup of a Liquid Jet in a Swirling Gas", *Physics of Fluids*, A, Vol. 2, pp.2134-2139, 1990.

[22] Lian, Y., Jeng, S. M., Jog, M. A., and Benjamin, M. A., "Advanced Sub-Model for Airblast Atomizers", *Journal of Propulsion and Power*, Vol. 17, pp. 411-417, 2001

[23] Dombrowski, N. and Johns, W. R., "The Aerodynamics Instability and Disintegration of Viscous Liquid Sheets", *Chemical Engineering Science*, Vol.18, pp.203-214, 1963.

[24] Rizk, N.K. and Mongia, H.C., "Model for Airblast Atomization", *Journal of Propulsion*, Vol. 7, pp. 305-311, 1991.

[25] Hilbing, J. H., and Heister, S. D., "Droplet Size Control in Liquid Jet Breakup", *Physics of Fluids*, Vol. 8, pp. 1574-1581, 1996.

[26] Mao, C. P., Chuench, S. G., and Przekwas, A. J., "An Analysis of Pressure Swirl and Pure Airblast Atomization", *Atomization and Sprays*, Vol. 1, pp. 215-235, 1991.

[27] Ibrahim, E. A., and Przekwas, A. J., "Impinging Jets Atomization", *Physics of Fluids A*, Vol. 3, pp. 2981, 1991.

[28] Marshall, A.W. and Di Marzo, M., "Modeling Aspects of Sprinkler Spray Dynamics in Fires", *Process Safety and Environmental Protection*, *Transaction of the Institution of Chemical Engineers: Par B,* Vol. 82, pp. 97-104, 2004.

[29] Watson, E. J., "The Radial Spread of a Liquid Jet over a Horizontal Plane", *Journal of Fluid Mechanics*, Vol. 20, pp.481-499, 1964.

[30] Liang, P. Y., and Ungewitter, R. J., " Modeling of Atomization and Secondary Breakup from First Principles", *Progress in Astronautics and Aeronautics*, Vol. 171, pp. 481-505.

[32] Chen, Y. S. Huan-Min, S., Chen P. C., and Wang, T. S., "General Numerical model for Liquid Jet Atomization Applications", *Journal of Propulsion and Power,* Vol. 14, pp. 581-584, 1998.

[33] McGrattan, K., "Fire Dynamics Simulator (Version 4) Technique Reference Guide", *NIST Special Publication 1018*, 2004.

[34] Gatti, P. L., "Probability theory and mathematical statistics for engineers", New York, 2005.

[35] Reitz, R. D. and Diwakar, R., "Effect of Drop Breakup on Fuel Sprays", *SAE Technical Paper Series*, 860469, Feb. 1986.

[36] McGrattan, K., Forney G.,"Fire Dynamics Simulator (Version 4) User's Guide", *NIST Special Publication 1019*, 2004.

[37] Trelles, J., Mawhinney, J. R., DiNenno, P. J., "Characterization of a High-Pressure Multi-jet Water Mist Nozzle for the Purposes of Computationa; Fluid Dynamics Modeling", *Hughes Associates, Inc*., Baltimore, Maryland.

[38] Rdulf J. Schick, "An engineer's practical guide to drop size", *Spraying Systems Co.*

[39] Weber, Z., *Angew Math Mech.* Vol.11 pp 136-154, 1931.